PDC CUTTER WEAR AND TEMPERATURE MODELING

By

DOUGLAS BRIDGES

Bachelor of Science in Mechanical Engineering

Oklahoma State University

Stillwater, OK

2018

Submitted to the Faculty of the
Graduate College of the
Oklahoma State University
in partial fulfillment of
the requirements for
the Degree of
MASTER OF SCIENCE
May, 2020

PDC CUTTER WEAR AND TEMPERATURE

MODELING

Thesis Approved:

Dr. Geir Hareland

Thesis Adviser

Dr. Prem Bikkina

Committee Member

Dr. Runar Nygaard

Committee Member

ACKNOWLEDGEMENTS

I would like to thank my advisor, Dr. Geir Hareland, for all of his help during my time completing this research. His guidance on this project kept me on track, while allowing me to complete the work as I had seen fit. Without him and his expertise in the drilling area, this project would not have been possible.

Dr. Prem Bikkina and Dr. Runar Nygaard, thank you for acting as committee members and for taking time to review my thesis.

Thank you to Sandia National Laboratories and David Raymond for supplying data that was used for this study.

I would also like to thank all members who were on this team from Oklahoma State University, University of Oklahoma and those working at Sandia National Laboratories. I would specifically like to thank Amin Atashnezhad for all of his input, guidance and previous work that helped me complete this project. Also, my fellow lab member, Seth Sleeper, thank you for keeping me sane for all the long commutes and always being willing to discuss my project.

Thank you to my family and my fiancé for their support throughout this journey. They have all supported me more than they ever knew and I would not have been able to achieve this without their help.

Last, I would like to dedicate this to my father. He believed in me even in times when I did not. I love you.

Name: DOUGLAS BRIDGES

Date of Degree: MAY, 2020

Title of Study: PDC CUTTER WEAR AND TEMPERATURE MODELING

Major Field: PETROLEUM ENGINEERING

Abstract: Since Polycrystalline Diamond Compact (PDC) drill bits have been developed, they have made a strong introduction into the drilling industry due to their tendency to produce a higher rate of penetration (ROP) than that of a rollercone. Even though a PDC bit is often times more efficient, the effects of bit wear still decrease PDC bit life. For both geothermal wells and oil/gas wells, bit wear has been a coherent setback during the drilling process since the beginning. Drilling a well efficiently is the key to being profitable and bit wear is a key factor in drilling efficiency. The research presented within, includes single cutter testing preformed at varying operating parameters to analyze effects on PDC wear rates and temperature development under the cutter wearflat. Previous temperature modeling is verified with single cutter data. From the single cutter data, significant differences are seen when wear surpasses the PDC layer. Based on these finding, a Differential Evolution Algorithm (DEA) optimization is used to calibrate a wear model based on PDC wear rates only. The wear model is applied to two separate bit runs to verify that it can predicts real-time wear based on operating parameters and rock properties. Using a detailed cutter geometry outlined in this study, wearflat temperatures and PDC temperatures are estimated on both bit runs. With the models outlined in this study, optimal operating ranges for weight on bit (WOB) and RPM can be achieved to limit PDC bit wear. The ultimate goal of this study is to combine this research with other individual for Oklahoma State University, University of Oklahoma, and Sandia National Laboratories to develop a real time drilling model. This research can be applied to any drilling application to increase efficiency by minimizing PDC drill bit wear.

TABLE OF CONTENTS

Chapter Page

LIST OF TABLES

Table Page

LIST OF FIGURES

Figure Page

Figure Page

NOMENCLATURE

Abr	*lithology relative abrasiveness*	-
A_w	*cutter wearflat area*	cm^2
å	*rotational speed exponent*	-
BG	*bit grade*	-
BG_C	*carbide bit grade*	-
BR	*back rake*	º
CCS	*confined compressive strength*	*psi*
C_a	*bit wear coefficient*	-
$C,\ C_1,\ C_2$	*constants*	-
d_b	*bit diameter*	*in*
D_c	*cutter diameter*	*in*
F_D	*dimensionless drilling rate group*	-
F_{NS}	*normal force on slider*	*lb*
F	*weight on cutter*	*N*
f	*thermal response function*	*J/kg • ºC*
G	*model constant*	-
GR	*gamma ray*	-
K_{hf}	*rock thermal conductivity*	*W/cm • ºC*
k_{wf}	*wear function constant*	-
K	*friction coefficient between cutter and rock*	-
$L_{Carbide}$	*length of thickest point of carbide wear*	*in*
L_{PDC}	*PDC thickness*	*in*
L_w	*cutter wearflat length*	*cm*
L	*length of cutting or sliding*	*ft*
N	*rotational speed*	*rev/min*
N_{st}	*standard rotational speed*	*rev/min*
n	*number of cutters*	-
P_O	*Overburden Pressure*	*psi*
q	*frictional heat flux into cutter*	W/cm^2
ROP_{st}	*standard rate of penetration*	*ft/hr*
ROP	*rate of penetration*	*ft/hr*
S	*confined compressive strength*	lb/in^2
STT	*sonic travel time*	*µsec/ft*
T_b	*bit torque*	*ft • lb*
T_D	*dimensionless torque group*	-
T_{fl}	*fluid temperature*	ºC

$\bar{T}_w$	*mean cutter wear flat temperature*	*ºC*
UCS	*unconfined compressive strength*	*psi*
U_D	*dimensionless cutter wear function*	-
V_C	*carbide worn volume*	*in³*
V_D	*volume wear of diamond*	*in³*
V_{PDC}	*PDC worn volume*	*in³*
V_R	*volume of rock removed*	*in³*
V_{sand}	*volume fraction of sand*	-
V_{sh}	*volume fraction of shale*	-
V_s	*volume wear of slider*	*in³*
V_T	*total worn volume*	*in³*
WOB_{st}	*standard weight on bit*	*lbs*
WOB	*weight on bit*	*lb*
$W_f =$	*bit wear function*	-
$w =$	*instantaneous bit wear*	-
$X_i =$	*incremental depth*	*ft*
$X =$	*length of worn PDC face*	*in*
$Y =$	*fractional bit wear*	-
$v =$	*cutting speed*	*m/s*
$\alpha_0 =$	*normalized rock quartz content*	-
$\beta =$	*abrasive constant*	-
$\Delta V =$	*volume of cutter removed*	*in³*
$\eta =$	*rock thermal diffusivity*	*cm²/s*
$\rho =$	*model constant*	-
$\sigma_o =$	*unconfined compressive strength*	*lb/in²*
$\tau =$	*model constant*	-

CHAPTER I

INTRODUCTION

In times when drilling rate of penetration (ROP) with Polycrystalline Diamond Compact (PDC) drill bits is key in order to reduce the cost of drilling, a reduction of weight on bit (WOB) or revolutions per minute (RPM) may be advised. With a real time calculation on polycrystalline diamond compact (PDC) bit wear, a more accurate interpretation recommendation of the operating parameters can be derived. While increased bit wear can allow for an increase in the range of WOB and/or RPM, the opportunity to increase ROP can be negated if the operating parameters are taken too far.

1.1 Motivation

The problem with PDC bits is that they constantly wear, from the time the bit begins to turn right up until it is pulled out of the hole. The best case would be to eliminate any and all wear, but since this is not possible, the next best thing is to reduce bit wear. There are many ways to reduce a bit's wear rate but not all cases are economical. In this approach, the real time measurement of overall bit wear and the thermal effect are taken into consideration when selecting real time operating parameters.

The reason for this research is to implement a real time drilling model based on the previous foot of drilled rock to give accurate operating ranges for the next foot of drilling. In order to properly gage the WOB and RPM ranges, accurate calculations of overall bit wear must be outlined and

likewise the PDC bit wear cutter temperature must be closely monitored to limit accelerated wear due to excess temperature rise.

Furthermore, this research is being done in conjunction with Oklahoma State University, University of Oklahoma and Sandia National Laboratories (SNL) to develop a real-time drilling optimization system for geothermal drilling. Along with the research preformed in this study on PDC bit wear and wearflat temperatures, there has been work completed on; drill stem vibration, Mechanical Specific Energy (MSE) and PDC ROP modeling and analysis. The overall goal can be visualized as a drilling parameter map seen in Figure 1.

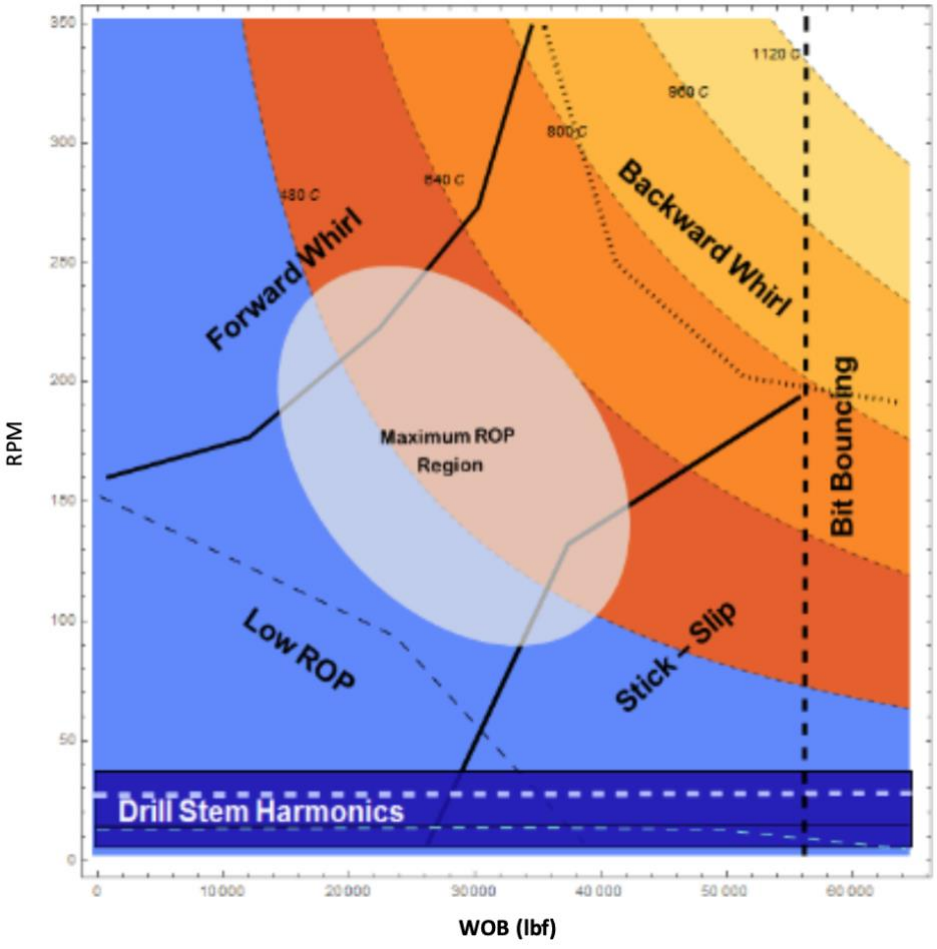

Figure 1: Real time ROP (or MSE) contour map

This is a visual representation of the optimum range of WOB and RPM to achieve the greatest ROP for the next foot to be drilled in real time. Remaining within the maximum ROP region would ensure the best drilling performance while minimizing drill string vibrations and accelerated bit wear due to increased temperatures.

1.2 Drill Bit History

Since the beginning of petroleum exploration, multiple types of drill bits have been used. From the Chinese Chisel type bits (Way, 1916), used for producing brine, to the modern-day rollercone and drag bits. Currently the rollercone and drag bits are the two main drill bit types being used in drilling operations. The separating factor between rollercones and drag bits is that rollercones have rotating cones and the drag bits have no moving parts which results in a different rock cutting mechanism during drilling.

Figure 2: Rollercone insert bit (right) and milled bit (left)

A rollercone, shown in Figure 2, has multiple cones that are attached with bearings and each cone has the ability to rotate around its own center. When a force is applied to the rollercone and the drillstem begins to rotate, the cones rotate due to the rock bit interaction friction and simultaneously crush the rock beneath the bit teeth. Rollercones are known to be successful in all

types of formations and are inexpensive compared to most drag bits. The downfall to the rollercone bit in most formations is decrease in ROP due to faster bit wear and low wear resistance which gives shorter bit runs, or mechanical failure due to worn bearings.

The term drag bit incorporates any fixed bit with no moving parts, meaning that the bit rotation is only due to the rotation from the drillstem and/or a down hole motor. There are many different types of drag bits but the most common are Polycrystalline Diamond Compact (PDC) bits, which can be seen in Figure 3. These PDC bits are typically cast or machined and then cutters are inserted into the body. Figure 4 shows the many different cutters shapes and sizes used in PDC bits, but most common cutters are cylindrical. The PDC cutters have a layer of diamond crystals that comes into contact with the rock and is intended to do the majority of the work. Unlike rollercone bits, PDC bits do not crush the rock, instead the PDC bit typically shears the rock off by sliding against it. Due to the nature of this review, the focus from here forward will be on PDC bits.

Figure 3: PDC bit

Figure 4: PDC cutter geometries

1.3 Bit Wear Overview

Although the technology has come a long way, there is one thing that all drill bits have in common, which is bit wear. In short, the drilling process is a combination of force and rotation and bit wear is caused by the interaction between the rock being drilled and the cutters that are attached to the drill bit itself. This interaction is a reaction of the compressive force through the drill stem or weight on bit (WOB) and the rotation (RPM) caused by a motor and/or applied to the drill stem at the surface. The WOB and RPM are both recorded variables during the drilling process, but the effect that these have while drilling is wear and bit wear is not as easily determined. The effects of PDC cutter wear is seen in Figure 5 for different stages of PDC cutter wear from laboratory testing.

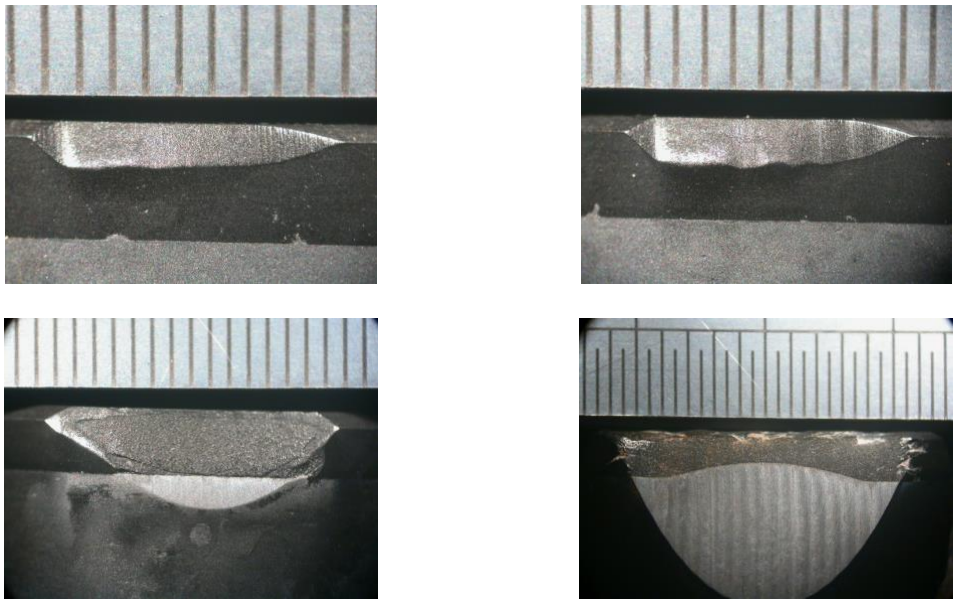

Figure 5: Bit wear after 30(top left), 60(top right),180(bottom left) and 360 min (bottom right)

One of the main reasons for trying to model bit wear or find ways to reduce bit wear is because of the drilling cost resulting from bit wear. Besides the upfront cost of the drill bit, the overall cost is also affected by the total depth drilled by each bit. This is where bit wear has a huge impact on

the drilling industry. It might be possible to achieve a minimal bit wear by decreasing the rate of penetration (ROP) and achieving a long run with a single bit but it would not be economical because of the drilling rig day rate. On the other hand, it is possible to maximize the ROP by increasing the WOB and RPM as high as possible, but the increased wear on the bit will decrease the life of the bit causing more bits to be used to reach the required depth. The formula that the industry is trying to achieve is somewhere in the middle. A formula that maximizes ROP while minimizing bit wear for an outcome that drills faster and longer. An array of research has been completed to try and find the best way to measure wear on all types of drill bits.

For the past 40+ years, multiple approaches have been implemented to improve drilling efficiency. When it comes to increasing drilling efficiency with the bit/cutters themselves, variables such as material (Wong et al., 2016) or design (Rahmani, 2019) have all been tested for improvements. In this review, we will not be discussing the effects of material or design, but the effect that the bit wear imposes on drilling efficiency. More specifically, we will be looking at the bit wear on PDC bits. Although drilling mechanics of a PDC cutter are easier to evaluate compared to that of a rollercone, a large range in performance is seen due to the variance in PDC design. By looking at previous research, this study will cover how PDC bits wear, how wear has been modeled and how the thermal effects can accelerate PDC bit wear.

CHAPTER II

THEORY

It has been known that PDC bits are much more efficient than the rollercone bits, but this is traditionally only seen while drilling soft rocks. This could be due to the fact that 50% of the energy for drilling can be dissipated by a worn cutter. (Geoffroy, Minh, Bergues, & Putot, 1999) In Geoffroy et al. (199), all the forces on a single cutter were simplified down into two forces. The cutting force, which is seen by the face of the cutter, and the frictional forces which are seen on the wear flat area beneath the cutter. With an increased wear flat, the cutting force must be increased to offset the frictional forces that incur.

In addition to the wear that is caused by the interaction between the rock and cutter, thermal effects can accelerate the rate at which a cutter will wear. When the study of thermal effects on PDC wear began, 750ºC was the maximum safe operating temperature. This temperature was established due to the fact that below this temperature microchipping was the wear seen on the cutter. Above 750ºC full diamond grains were being removed from the diamond layer and when reaching temperatures above 950ºC the tungsten carbide stud experienced plastic deformation (Ortega & Glowka, 1984). The understanding of the cutters and PDC bit geometry must be precise to provide adequate information when making a bit selection. Due to this, a PDC bit model is a combination of the geometry of cutter placement within a bit the single cutter force

and wear models. A single cutter model is used for predicting the forces and accumulated wear on a single cutter but do not account for a cutters position within a whole bit which includes multiple cutters in many different locations on the bit. Warren and Sinor (1986), incorporated theories from single cutter models to achieve a PDC bit model. Lab tests of different types were conducted to look at the different outcomes for new bits, worn bits and bits with cutters removed. Three separate tests on new bits were conducted in Carthage limestone, Berea sandstone and Catoosa shale. The model calculations for these tests matched the data when relating WOB and ROP. These tests were also conducted with worn bits and the model predictions were once again a good match for the associated WOB versus ROP. The model developed by Warren and Sinor (1986) also predicted that by removing cutters the ROP would increase for any given WOB. ROP for bits with new cutters did not change when cutters were removed but the data did show that ROP increases when bits with slightly worn cutters had cutters removed. The model predicted this increase in ROP, but the model underestimated the increase by nearly 50% for the case stated above.

2.1 PDC Wear Models

One of the first models that claims to have derived a function for instantaneous bit wear was from (Kuru & Wojtanowsicz, 1988). In this model, there are four steps that can be followed to calculate the current bit wear and any change in lithology while drilling. The four-step process is started by calculating dimensionless torque, T_D, and a dimensionless drilling rate group, F_D.

$$T_D = \frac{12T_b}{WOBd_b} \qquad \text{Eq. 2.1}$$

$$F_D = \frac{12\left(\frac{ROP}{ROP_{st}}\right)}{\left[U_D\left(\frac{WOB}{WOB_{st}}\right)\left(\frac{N}{N_{st}}\right)^{\hat{a}}\right]} \qquad \text{Eq. 2.2}$$

T_D vs. F_D is then extrapolated as a straight line from the drilling data (WOB, bit torque, ROP and RPM) and can be used as a marker to detect any changes in the lithology. A change can be

assumed if any instantaneous T_D vs. F_D calculations deviate from the straight-line plot. The instantaneous bit wear is then calculated by taking the current T_D and using this information to back solve for the dimensionless cutter wear function, U_D, from the T_D vs. F_D straight line plot. U_D can be used to solve for y(w) where w is the instantaneous bit wear (Kuru & Wojtanowsicz, 1988).

$$U_D = \frac{\sqrt{y + \frac{1}{3}y^2} * (y - 5^2 + 8y^3 - 4y^4}{\left(1 + \frac{2}{3}y\right) * \sqrt{y - 5y^2 + 8y^3 - 4y^4} - \sqrt{y + \frac{1}{3}y^2} * (1 - 10y + 24y^2 - 16y^3)} \quad \text{Eq. 2.3}$$

$$y = w + 0.028e^{-.05w} \quad \text{Eq. 2.4}$$

With the assistance of a computer program, the instantaneous bit wear could be derived from recording the initial drilling data and following the procedures to back out the current wear of the bit.

A novel approach was taken by Appl et al. (1992), by using a simplified model for bit wear. To easily get a grasp on the true mechanics behind bit wear a basic machining equation for sliding wear volume was considered. Sliding wear is defined by:

$$\frac{dV_s}{dt} = CF_{NS}\frac{dL}{dt} \quad \text{Eq. 2.5}$$

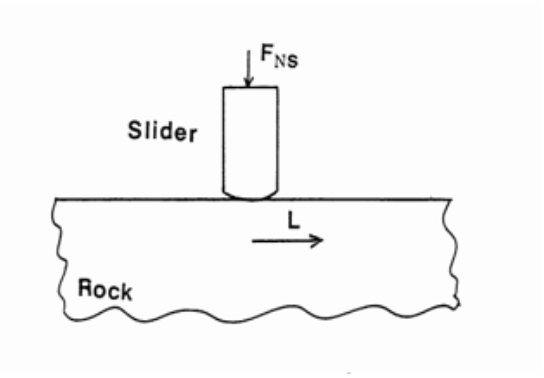

Figure 6: Sliding wear (Appl et al. 1992)

Based on this simple relation, Appl et al. (1992) derived an equation for the sliding wear flat volume:

$$\frac{dV_D}{dt} = C F_{NWD} \frac{dL}{dt} F(T) \quad \text{Eq. 2.6}$$

$$F_{NWD} = \sigma_o A_w \quad \text{Eq. 2.7}$$

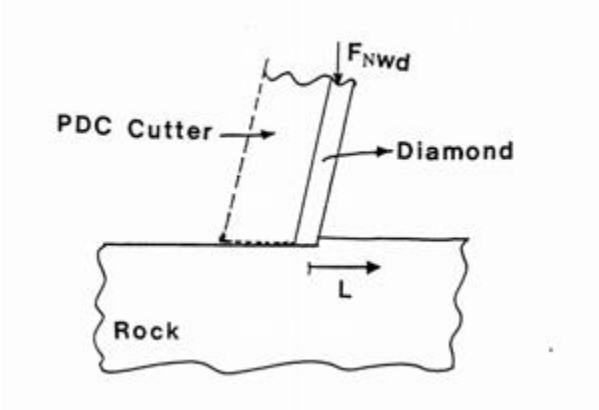

Figure 7: PDC sliding wear (Appl et al. 1992)

The volume of the rock removed can be defined as:

$$\frac{dV_R}{dt} = A_P \frac{dL}{dt} \quad \text{Eq. 2.8}$$

Combining Equation 2.6, Equation 2.7 and Equation 2.8 the relation of the diamond removed and rock removed will be:

$$\frac{dV_D}{dV_R} = C\sigma_o \frac{dL}{dt} F(T) \quad \text{Eq. 2.9}$$

Based on these equations bit wear can be calculated based on the ROP that is being achieved during the drilling process. It is implied that wear is a function of temperature ($F(T)$) but the

literature does not expand on this function, consequently it is an unknown. So, although it is known to have an affect it is not fully explained to verify this model.

ROP is known to be directly affected by the wear that is attained while drilling. In the Motahhari et al. (2010) paper on drilling efficiency, a non-dimensional wear function is included in a ROP model. The ROP of a PDC bit with perfect cleaning is:

$$ROP = W_f * G * \frac{WOB^a * N^b}{S * d_b} \quad \text{Eq. 2.10}$$

where W_f is the wear function. The wear function would be one for a new bit and decrease until the bit is fully worn resulting in a value of zero. Using experimental data from Glowka (1987), an estimate of wear was developed by Motahhari et al. (2010). The equation for the wear function is:

$$W_f = k_{wf}(\frac{WOB}{n})^{\rho} \frac{1}{S^{\tau} * A_w^{\rho+1}} \quad \text{Eq. 2.11}$$

from these two equations (Eq. 2.10 and Eq. 2.11), the ROP and W_f can be calculated for a given set of drilling parameters but do not result in the actual bit wear. Motahhari et al. go on further to derive an equation (Eq. 2.12) that sums up the infinitesimal volumes removed:

$$\Delta V = C_a \sum_{i=d_{in}}^{d_{out}} \left(\frac{WOB_i}{1000n}\right)^{C_1} * RPM_i^{C_2} * \frac{S_i}{1000} * Abr_i \quad \text{Eq. 2.12}$$

With this equation, the total volume removed from a cutter can be continuously calculated during drilling. With an actual model for volume wear, a more accurate calculation for ROP can be completed and a bit can be pulled before damaging a bit.

In a report by Liu et al. (2014), it is claimed that Equation 2.12 contains too many constants and coefficients, therefore making it problematic to use for actual applications. A new bit wear model was then proposed by Liu et al. to try and reduce the number of unknowns and make it more relevant to actual applications. This new model is:

$$\Delta V = \beta * \alpha_0 * S * F_a * L \quad \text{Eq. 2.13}$$

In the Equation 2.13, β is a constant that is based on the rock and cutter properties, S is the rock strength, F_a is the axial force applied to the cutter, L is the cutter sliding distance and α_0 is the rock quartz content and can be estimated using the following equation (Eq. 2.14),

$$\alpha_0 = 0.1 * V_{sh} + 0.8 * V_{sand} \quad \text{Eq. 2.14}$$

To further expand on wear the paper derives an equation for fractional bit wear that will help when calculating bit grade, ΔBG, or a value for the wear function, W_f. The fractional bit wear is:

$$Y_i = \sqrt[3]{\frac{\pi}{3.2}\frac{\beta}{V_0}\frac{D_b^2}{G}\frac{\alpha_{0i}S_i^2X_i}{(1-Y_{i-1})} + Y_{i-1}^3} \quad \text{Eq. 2.15}$$

From here Y_i can be used to calculate the wear function and bit grade:

$$W_f = 1 - Y_i \quad \text{Eq. 2.16}$$

$$\Delta BG = 8Y_i \quad \text{Eq. 2.17}$$

Although this model appears to be easier for actual applications, the downfall is that it assumes the volume lost is that of an inverse pyramid which can be seen in Figure 8. This assumption reduces the cutter volume lost directly affecting the wear function and bit grade calculations.

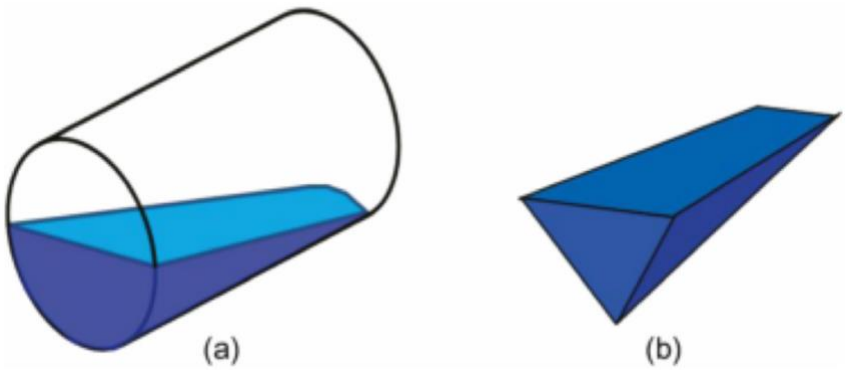

Figure 8: PDC worn volume assumption (Liu et al., 2014)

2.2 Thermal Effects

If thermal effects were neglected, it could be concluded that bit wear was simply just a function of the load applied to a bit and the distance traveled while in contact with the rock. As we previously discussed though, this is not the case and thermal effects have a large impact on the rate at which bits wear. In Glowka's (1986) stated that abrasive wear of metal is related to the ratio of the relative hardness of the abrasive material and that of the metal. For soft abrasives, with a ratio less than 1.2, the wear rate is typically low. As the ratio of relative hardness exceeds 1.2, the wear rate increases considerably. When looking at quartz, which is anywhere from 20-40% of many rock formations, the hardness ranges between 9.8-11.3GPa and that of tungsten carbide is 10-15GPa. These ranges result in a ratio that range from 0.65-1.13, classifying this relationship as a soft abrasive. From testing it is seen that when tungsten carbide is used for cutting rocks at or below 350 ºC, they experience a wear rate that is similar to that of a soft abrasive as expected. When the temperature exceeds 350 ºC, wear is accelerated and associates better with that of a hard abrasive. From this, Glowka et al. (1986) concluded that wear increases by thermal effect. To reduce PDC wear it would be advantageous to control the temperature of the cutters. This is found to be possible by using proper WOB and RPM applied to the bit. Two-dimensional finite element modeling was conducted on a single cutter model to determine the thermal response of a PDC cutter at the rock and cutter interface. From this, a thermal response function was derived and incorporated into a wear model. The equation for the mean temperature of a cutter wear flat is the following

$$\bar{T}_w = T_{fl} + \frac{KFvf}{A_w\left[1 + \frac{3\pi}{4}K_{hf}f\left(\frac{v}{\eta L_w}\right)^{\frac{1}{2}}\right]} \qquad \text{Eq. 2.18}$$

This equation is a function of the force applied to the cutter and the speed at which the cutter is sliding across the surface of the rock. Rearranging this equation to solve for a critical force, F_{cr}, which is the force that is associated with the temperature that exceeds a soft abrasive reaction.

$$F_{cr} = \frac{A_w(\bar{T}_w - T_{fl})\left[1 + \frac{3\pi}{4} K_{hf} f \left(\frac{v}{\eta L_w}\right)^{\frac{1}{2}}\right]}{Kvf} \quad \text{Eq. 2.19}$$

With these equations, the correct parameters can be determined to remain within an optimal range to mitigate excessive temperatures and ultimately increase the life of a bit if the current wear relations, A_w and L_w, are known.

One area that was not defined well in Glowka's earlier studies was the thermal response function, f. Glowka (1987) defines f as;

$$f = \frac{\bar{T}_w - T_{fl}}{q} \quad \text{Eq. 2.20}$$

where q is the input heat flux or heat flux received by the cutter. The Sandia report goes into detail about the value of f for multiple different cutters that were used during the testing but were all computed using finite element analysis (FEA). Without performing FEA for each new cutter it could be very difficult to compute an accurate f value for use when calculating T_w or F_{cr}. The Sandia report lists f values for mildly worn cutters from 0.026-0.956 and for severely worn cutters from 0.166-5.459 depending on the convective heat transfer coefficients. For cutters that are similar in geometry and wear area to those used in the Glowka studies, values for f could be accurate but as the geometry or wear area change the values for f might be skewed. (Glowka, 1987)

2.3 Hypothesis

In hard rock drilling conditions, bit wear is a large player in the overall efficiency of a project. With excessive wear comes extra trips in and out in order to replace worn bits. When the overall

economics of a well can be affected by the capital expenditure of drilling, bit wear can be a deciding factor when it comes to a well being economic or not being economic. Based on these premises, this is the foundation of this study. By accurately measuring PDC wear and remaining within operating parameters to mitigate excessive wear due to excessive temperatures, more footage can be drilled between trips resulting in reduced cost and a better overall economic outcome for a well.

The scope of this study will be first and foremost to find a method to accurately calculate/predict volumetric PDC bit wear. Along with bit wear as a function of operating parameters, this study will focus on the thermal effect that can arise due to extreme operating conditions and the outcome will propose a method to limit this excessive wear.

CHAPTER III

METHODOLOGY

As the main focus of this study is the PDC wear that is accumulated during the drilling process, a method of simulating drilling to acquire accurate data acquisition must be used. In this study, a Vertical Turret Lathe (VTL) as seen in Figure 9, was used to simulate drilling with the single cutter method all of which was performed by a third party.

3.1 Single Cutter Testing

Figure 9: Vertical Turret Lathe (VTL)

In order to best mimic the likes of an actual drilling situation, many multi-strength rock samples had been developed. These multi-strength rock samples have consisted of mixing multiple rock types and cementing them together, creating layers of rocks with different strengths or putting together a “rock pie” as seen in Figures 10 and 11. The final decision was to use the rock pie consisting of Yellow Torrey Buff Sandstone, Red Sandstone and Texas Pink Granite. This rock pie was then placed on the VTL for single cutter dry testing, which is displayed in Figure 12.

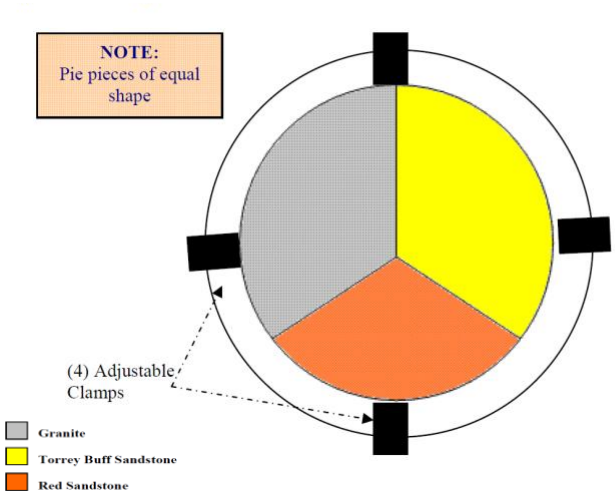

Figure 10: Rock pie set-up configuration

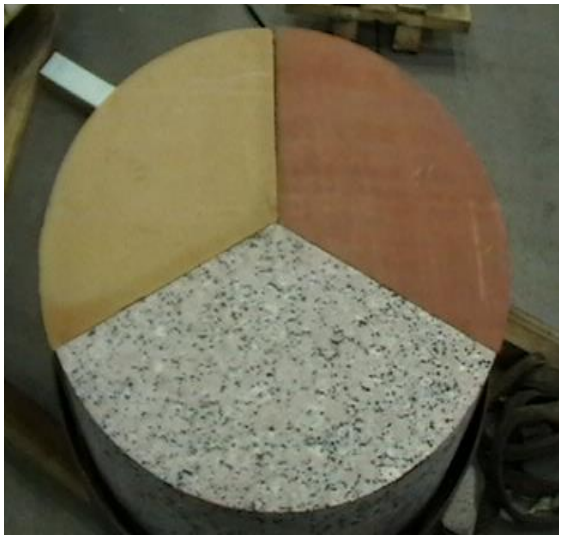

Figure 11: Completed rock pie

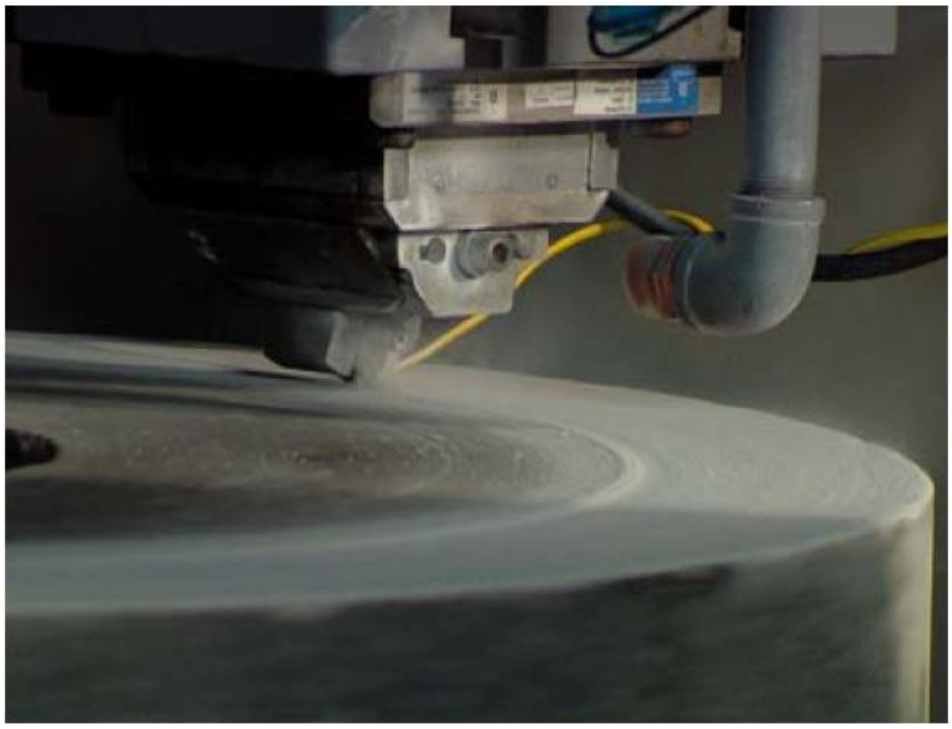

Figure 12: Single cutter dry testing

The equipment used during testing was the VTL, a 3-axis dynamometer and the LabVIEW software for recording all data during the testing. The conglomerate rock pie consisted of one third Yellow Torrey Buff Sandstone, one third Red Sandstone, and one third Texas Pink Granite. The rock pie was loaded onto the VTL and was machined across the top and along the outside diameter to ensure quality data acquisition.

For this study, multiple different single cutter tests were performed. In order to find relationship between PDC wear and drilling parameters, tests with varying WOB and RPM had to be conducted. For these procedures WOB was determined by altering the depth of cut (DoC) in 0.5 mm increments and the RPM was held at 75 or 125 for the duration of each test. Tests were conducted at 30, 60, 180 and 360 minutes for each variation and max force, temperature and volumetric wear were recorded at the end of each test.

All measurements for this study were recorded through the LabVIEW data acquisition system and can be seen in the table below. Although it was reported by the third party that the force applied

to the cutter was recorded throughout the duration of the test, access to these files was not granted. Max force values were generated by digitizing a graph that was found within the third-party literature used for this research.

Cutter #	Label	DOC (in)	RPM	Cutting Speed (ft/s)	Test Time (min)	Actual Time (min)	Cutter Volume Loss (in^3)	Wearflat Temperature (ºF)
1	1-50-75-30	1.97E-02	75	3.4	30	30	7.75E-06	428
2	1-50-75-60	1.97E-02	75	3.4	60	60	1.42E-05	527
3	1-50-75-180	1.97E-02	75	3.4	180	180	4.03E-05	617
4	1-50-75-360	1.97E-02	75	3.4	360	360	3.49E-04	711
5	1-50-125-30	1.97E-02	125	5.6	30	30	1.26E-05	518
6	1-50-125-60	1.97E-02	125	5.6	60	60	2.40E-05	518
7	1-50-125-180	1.97E-02	125	5.6	180	180	3.00E-04	673
8	1-50-125-360	1.97E-02	125	5.6	360	300	2.99E-03	788
9	1-100-75-30	3.94E-02	75	3.4	30	30	7.88E-06	455
10	1-100-75-60	3.94E-02	75	3.4	60	60	1.53E-05	482
11	1-100-75-180	3.94E-02	75	3.4	180	180	5.56E-04	644
12	1-100-125-30	3.94E-02	125	5.6	30	30	1.25E-05	500
13	1-100-125-60	3.94E-02	125	5.6	60	60	3.01E-05	491
14	1-100-125-180	3.94E-02	125	5.6	180	145	5.33E-03	788
15	1-150-75-30	5.91E-02	75	3.4	30	30	1.30E-05	527
16	1-150-75-60	5.91E-02	75	3.4	60	60	1.87E-05	500

Table 1: Recorded single cutter data

3.2 Differential Evolution For Wear Optimization

The data collected from the single cutter testing was used in conjunction with a Differential Evolution Algorithm (DEA). DEA is an optimization algorithm and is considered to be one of the most powerful tools for global optimization. The DEA is an optimization technique that was first developed by Storn and Price in 1997 to solve the Chebychev Polynomial fitting. The DEA is considered to be a simple population based, stochastic function minimizer; all while being robust and powerful. In simple terms, a population for the unknown variables are selected and computed. After a single computation is completed, at least one member of the population or variable is mutated and the computation is completed again. This mutation occurs over and over, for all variables for a set number of iterations. As the mutations continue, the algorithm converges at the local minimum or optimum outcome for the unknown variables. The purpose of the DEA in this study was to find a global optimization for bit wear. Parameter constants need to be found for WOB and RPM in the wear function to be used throughout this study.

3.3 Cutter Volumetric Wear Calculations

Often when modeling bit wear, a volumetric assumption is made, as discussed with the inverse pyramid that Lui et al modeled. To properly model real time bit wear, an accurate volumetric calculation must be available. The following equation, developed by Atashnezhad (2019), accurately solves for the total worn volume based on Bit Grade (BG). The derivation of this equation can be found in Appendix A and Figure 13 is a schematic of the cutter parameters.

$$V_T = -\left[\frac{(A)^3}{Tan(BR)}\left[\left(\frac{(A)-(B)}{(A)}\right) * \text{Cos}^{-1}\left(\frac{(A)-(B)}{(A)}\right) - \sqrt{1-\left(\frac{(A)-(B)}{(A)}\right)^2}\right]\right.$$

$$\left. - \frac{(A)^3}{3\,Tan(BR)}\left(\sqrt{1-\left(\frac{(B)-(A)}{(A)}\right)^2}\right)^3\right] \qquad \text{Eq. 3.1}$$

Where $A = \left(\frac{D_c}{2}\right)^3$, $B = \frac{BG*D_c}{8}$ and $BG = \frac{X*8}{16}$

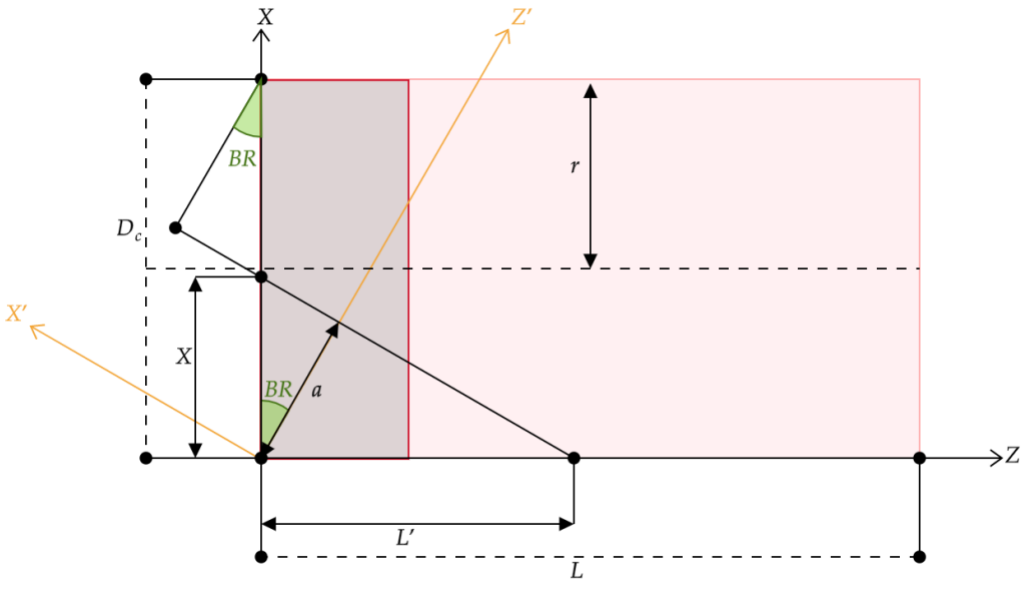

Figure 13: Schematic of cutter side view

Along with accurately calculating the overall wear of a PDC cutter, the need to calculate the PDC versus carbide wear is present in this study. As seen if Figure 14, the wear can surpass that of the PDC layer and reach the carbide layer of the cutter. Since the materials have different properties, and potentially wear at different rates, it is ideal to be able to calculate separate wear volumes for each.

Figure 14: Cutter wear- PDC only (left) and Combined PDC and carbide (right)

In order to calculate the PDC and carbide wear volumes a piecewise function must be utilized to calculate the carbide wear volume.

$$L_{Carbide} = L' - L_{PDC} \qquad \text{Eq. 3.2}$$

$$If\ L_{Carbide} \leq 0, \qquad V_{Carbide} = 0 \qquad \text{Eq. 3.3}$$

$$If\ L_{Carbide} > 0, \qquad V_C = -\left[\frac{(A)^3}{Tan(BR)}\left[\left(\frac{(A)-(B_c)}{(A)}\right) * \text{Cos}^{-1}\left(\frac{(A)-(B_c)}{(A)}\right) - \sqrt{1-\left(\frac{(A)-(B_c)}{(A)}\right)^2}\right] - \frac{(A)^3}{3\,Tan(BR)}\left(\sqrt{1-\left(\frac{(B_c)-(A)}{(A)}\right)^2}\right)^3\right] \qquad \text{Eq. 3.4}$$

$$Where\ A = \left(\frac{D_c}{2}\right)^3,\ B_c = \frac{BG_C * D_c}{8}\ and\ BG_C = \frac{L_{carbide} * 8}{\cot(BR) * D_C}$$

$$V_{PDC} = V_T - V_C \qquad \text{Eq. 3.5}$$

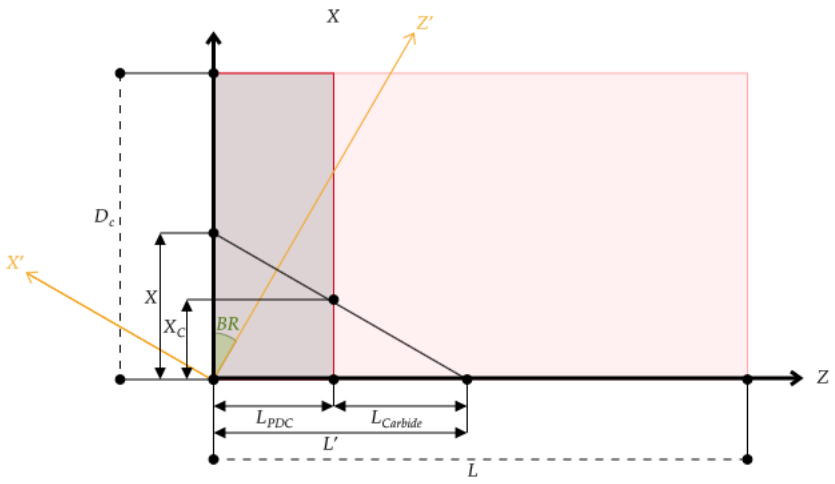

Figure 15: Cutter side view with PDC and carbide wear

From the above, Equation 3.4 gives the results for the carbide volume and with this Equation 3.5 can be used to give the PDC volume. Appendix A.2 gives further details on the calculations for the separate wear volumes.

3.4 Field Testing

The ultimate goal of this project, combined with the work of others, is to develop a real-time drilling optimization system. Single cutter data are pertinent to control variables while testing, but field testing can be used to verify findings and show how the work can be implemented.

3.4.1 Drilling Project

Sandia National Laboratories (SNL) completed a geophysical test hole, detailed in Raymond (2012), which had been sponsored by the US Navy Geothermal Program Office (GPO). The main goal of the GPO is to develop and manage geothermal resources on the Department of Defense lands.

The geophysical test hole was drilled on the Chocolate Mountain Aerial Gunnery Range (CMAGR), which is located along the eastern margin of the Salton Sea in Southern California. The test hole known as 17-8, is located in the northwest portion of the CMAGR. Figure 16 is a map of the test hole location.

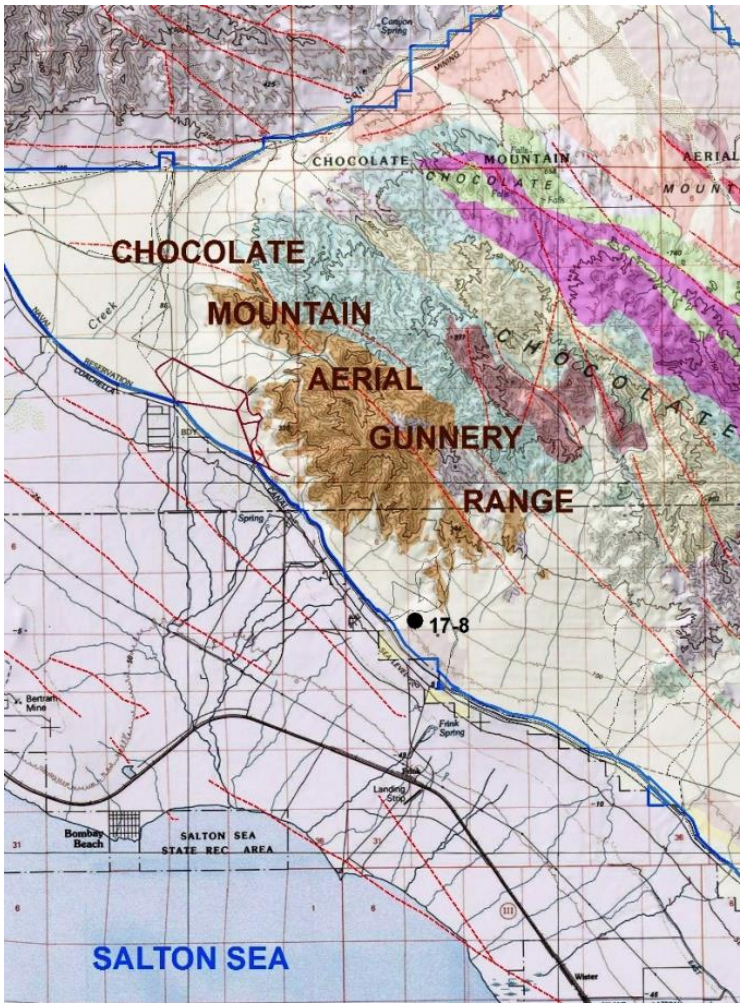

Figure 16: Geophysical Test Hole 17-8, Chocolate Mountains, CA (Raymond, 2012)

3.4.2 Drilling Data

The data received from test hole 17-8 consisted 13 time-based files for bit run #1, 11 time-based files for bit run #2 and a single depth-based file that included data for both bit runs. The time-

based files had recordings every second for all drilling data, including WOB and RPM. The depth-based file was in ½ foot increments and included gamma ray and sonic travel time which are used for calculating rock properties.

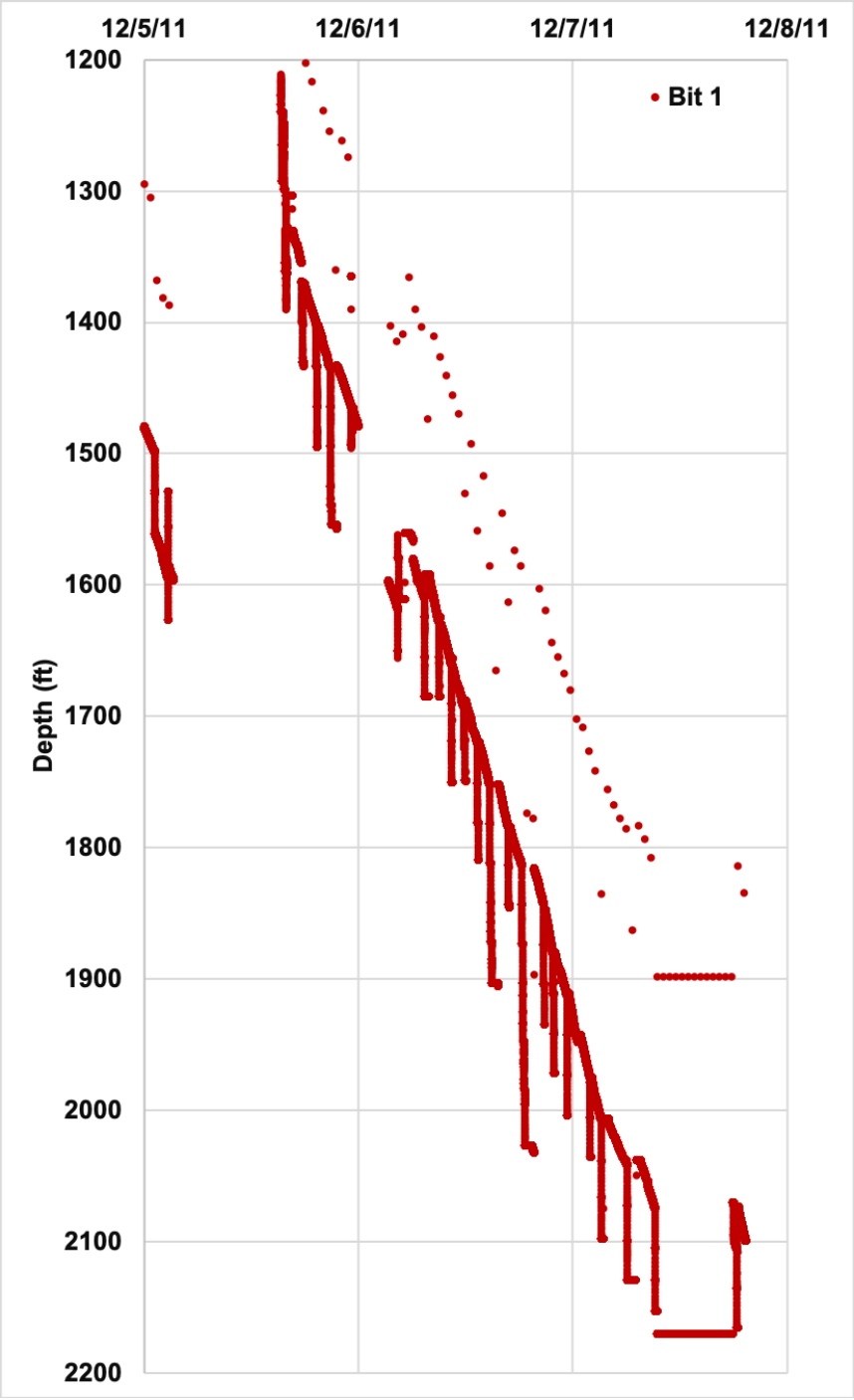

Figure 17: Raw CM Bit #1 depth plot

The ultimate goal with these data sets was to match the proper time-based file data with that of the depth-based files so that calculations including parameters from both could be completed. With a total of 14 files just for bit #1, a large amount of unwanted data, from tripping and non-rotating time, was included. Quality control (QC) of the data was a pertinent part of this project to ensure accurate end results. In order to begin work on the data, all 13 of the time-based files for bit run #1 were combined and can be seen in Figures 17 and 18. The figures show that there were discrepancies, not only in depth over time due to tripping, but also the starting time stamp of some of the files was incorrect.

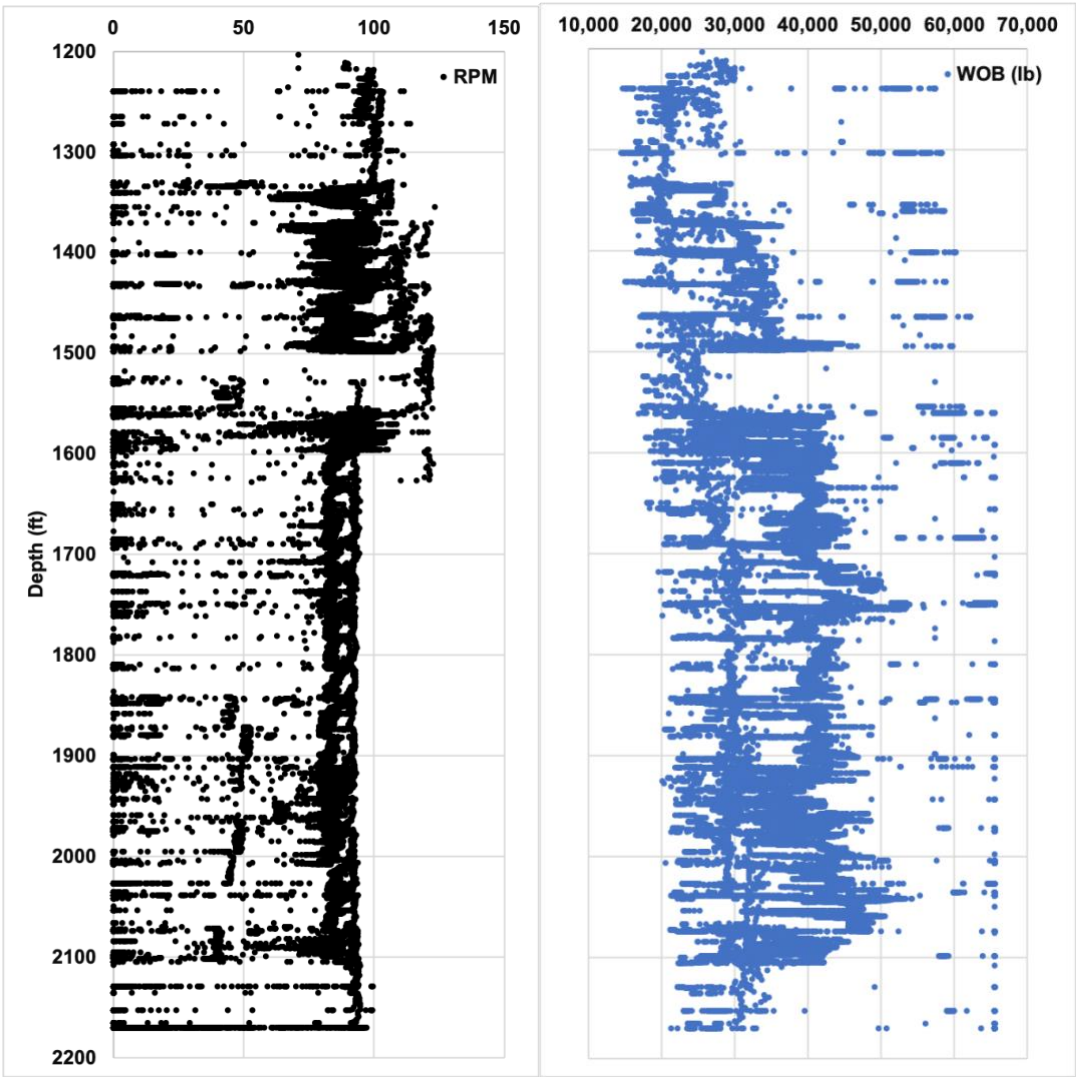

Figure 18: Raw CM Bit #1 operating parameters

After combining the files, the first step (phase 1) was to filter the data from tripping in and out of the hole. Figure 19 shows the depth vs time along with the operating parameters for the phase one of QC. When eliminating the tailing effect, seen when tripping or adding a drill pipe, the data cleans up but there are still some discrepancy in depths leaving a gap in the operating parameters. Along with the gap in the operating parameter, there are still some discrepancies in the timeframe and even some overlapping depths.

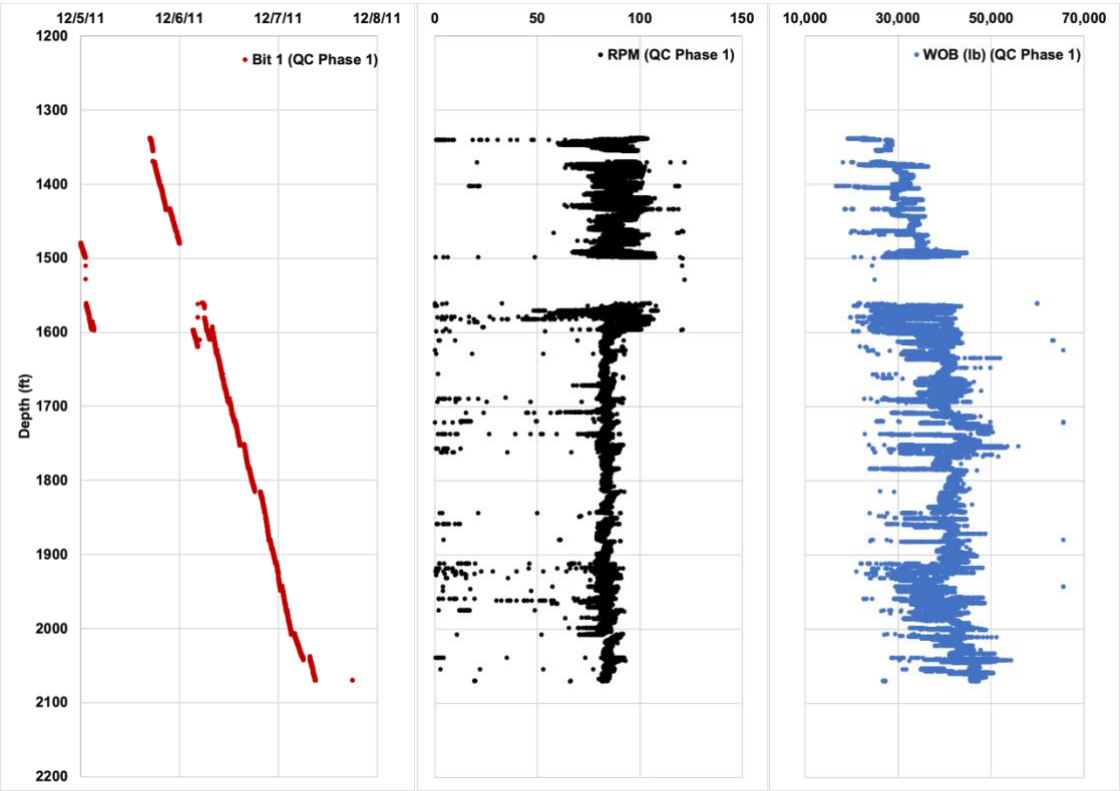

Figure 19: CM Bit #1 Data QC Phase 1

QC phase 2 consisted of correcting the time stamps and depths in order to get one continuous data set. As seen in the difference between Figure 19 and 20, a few of the data runs were brought forward so that the time sequence would be consecutive amongst the data. Also, when there were cases that the depths recorded overlapped with adequate operational data the overlaps were placed to run in sequential order with the nearest continuous data. By reordering the times to run

continuously and repositioning the depths that overlapped, a continuous depth based file was formed and can be seen in Figure 20.

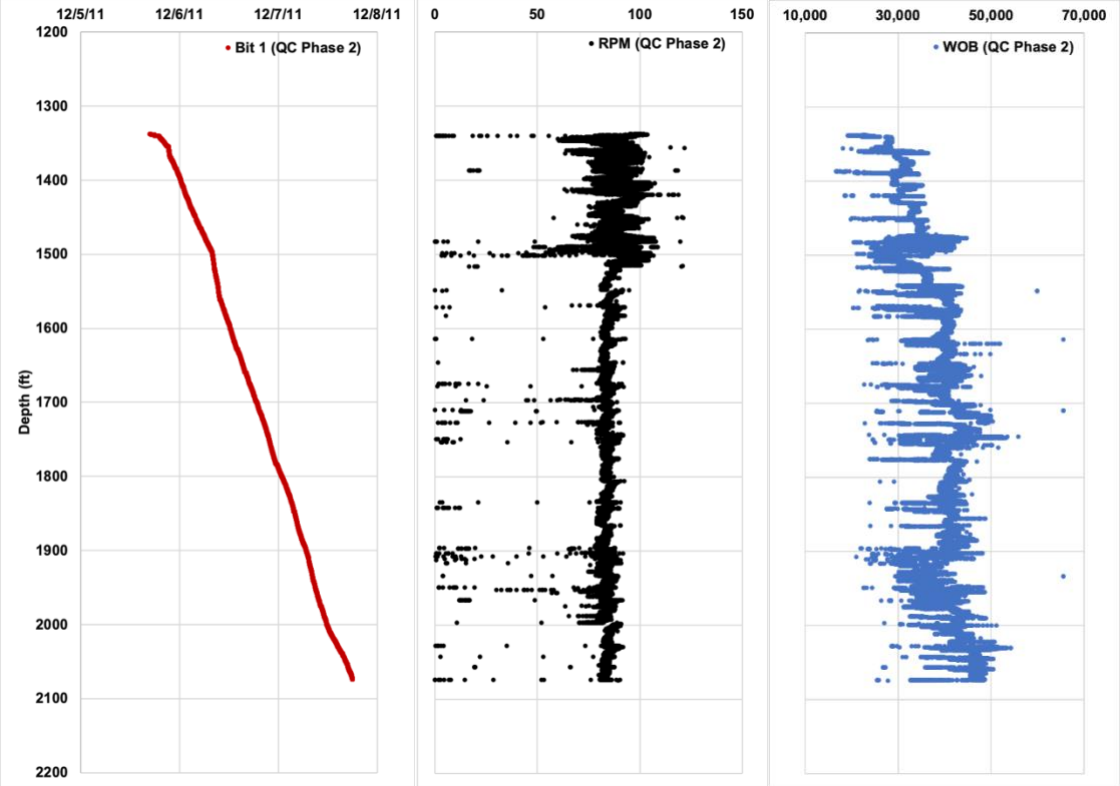

Figure 20: CM Bit #1 Data QC Phase 2

Although the time-based files had been arranged in progressive order based on depth after phase two, they still did not line up correctly with the single depth-based file. The data at the end of phase 2 had no consistent increase in depth while the depth files were stepped in ½ ft increments. In order to combine the files, the time-based files were rounded to the nearest ½ ft for depth and the operating parameters, RPM and WOB, were averaged over the steps to complete phase 3 of the QC process. These averaged parameters can be seen in Figure 21.

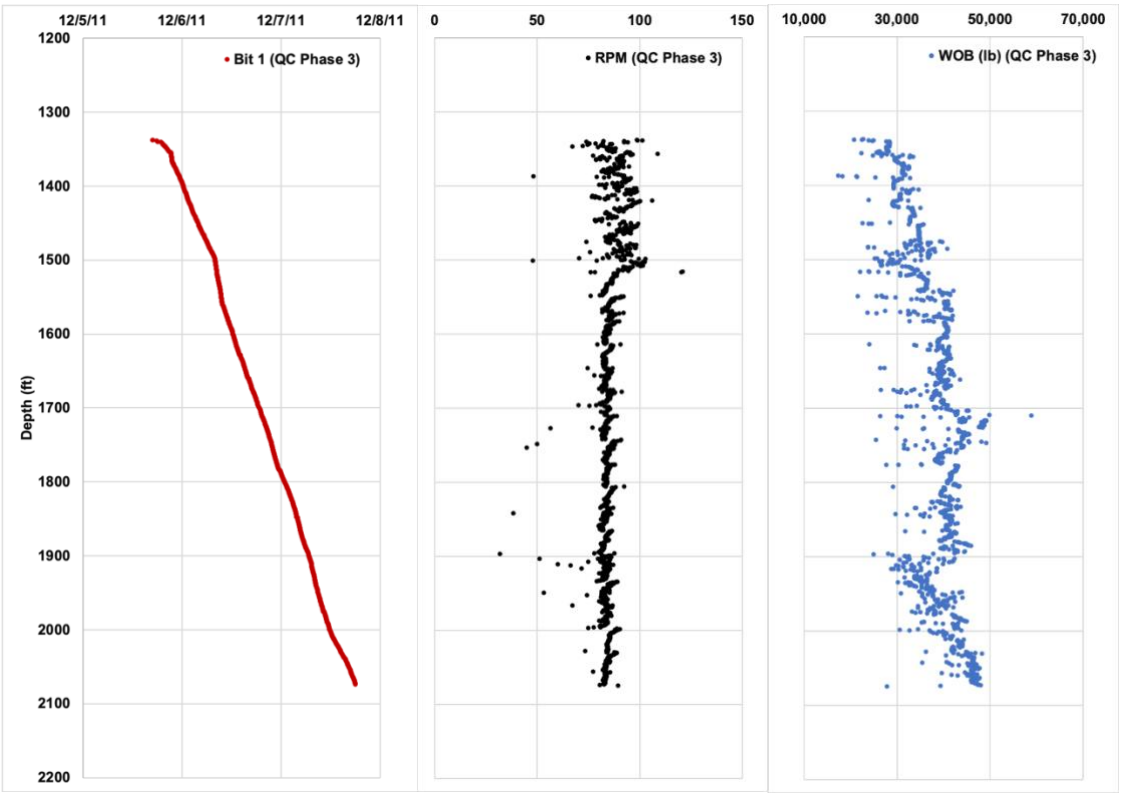

Figure 21: CM Bit #1 Data QC Phase 3

The next step in this process was converting the parameters from the depth based files, sonic travel time (STT) and gamma ray (GR) into usable parameters, confined compressive strength (CCS) and abrasiveness (Abr). To convert SST to unconfined compressive strength (UCS), a method developed by E.C Onyia was used. In Onyia's 1988 paper, the relationship is made between STT and UCS. The relationship is defined as

$$UCS = K_6 + \frac{K_7}{SST} \quad \text{Eq. 3.6}$$

Where K6 is -3.0444 and K7 is 881.1229. A graph showing the conversion can be found in Figure 22. Next, for UCS to CCS, Winters et al. (1987) was used to make the following correlation.

$$CCS = UCS(1 + 0.3 * (\frac{P_O}{145})^{0.7} \quad \text{Eq. 3.7}$$

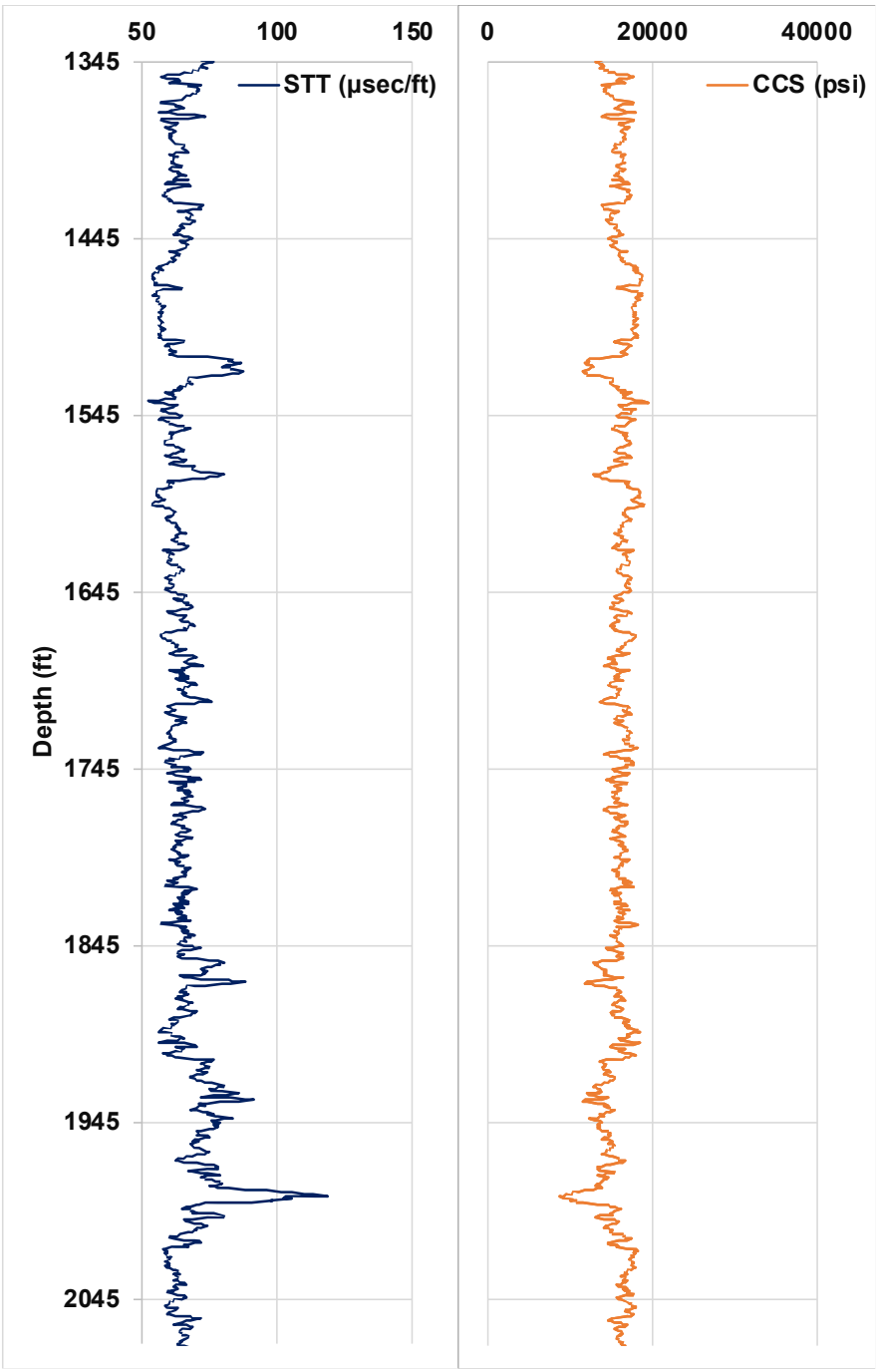

Figure 22: Conversion from sonic travel time to confined compressive strength

A piecewise function was used as a simple conversion from GR to Abr. Equation 3.8 was used for this correlation and the conversion can be seen in Figure 23

$$Abr = \begin{cases} 0.9; & if\ GR < 40 \\ -0.008 * GR + 1.22 \\ 0.1; & if\ GR > 140 \end{cases} \quad \text{Eq. 3.8}$$

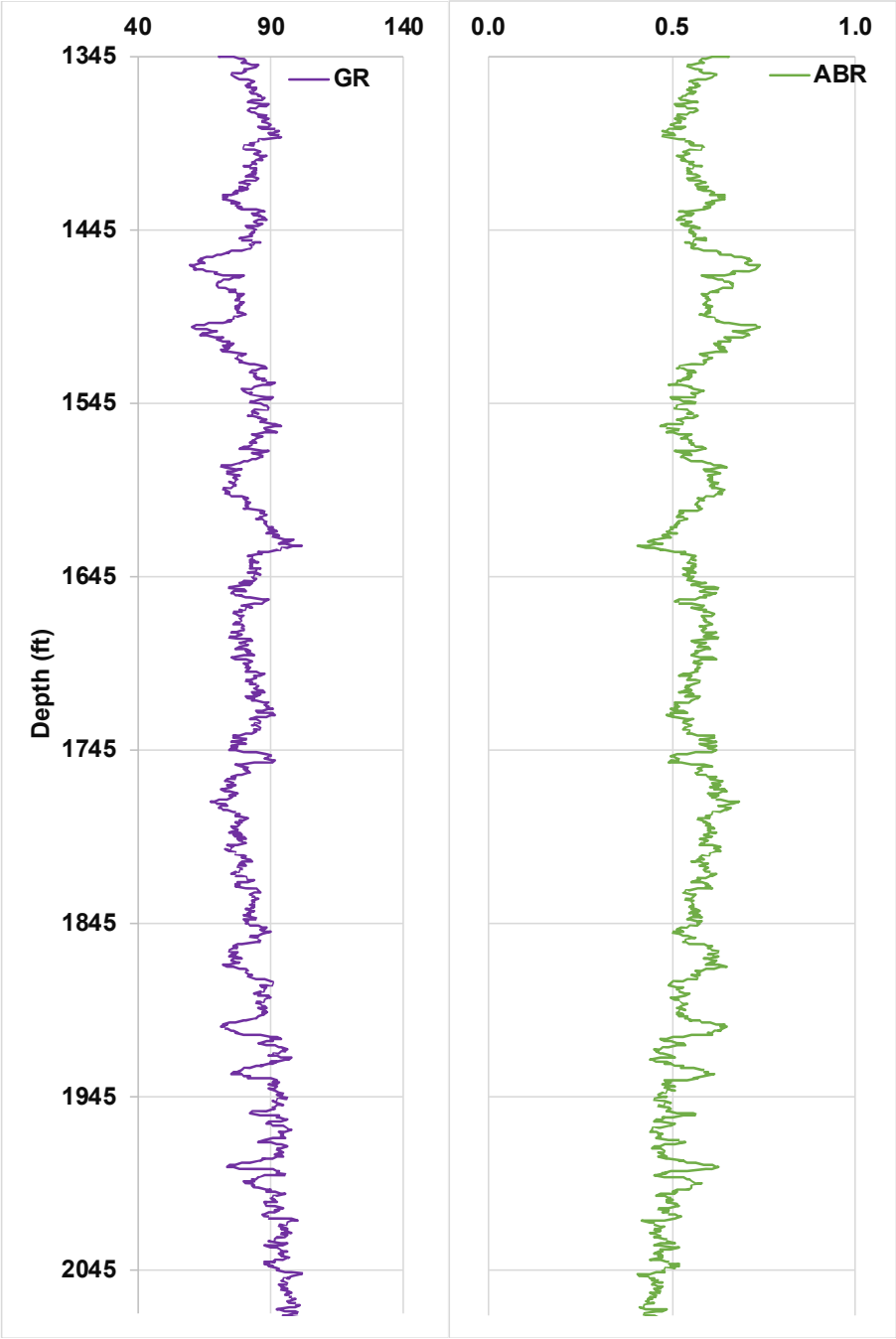

Figure 23: Conversion between gamma ray and abrasiveness

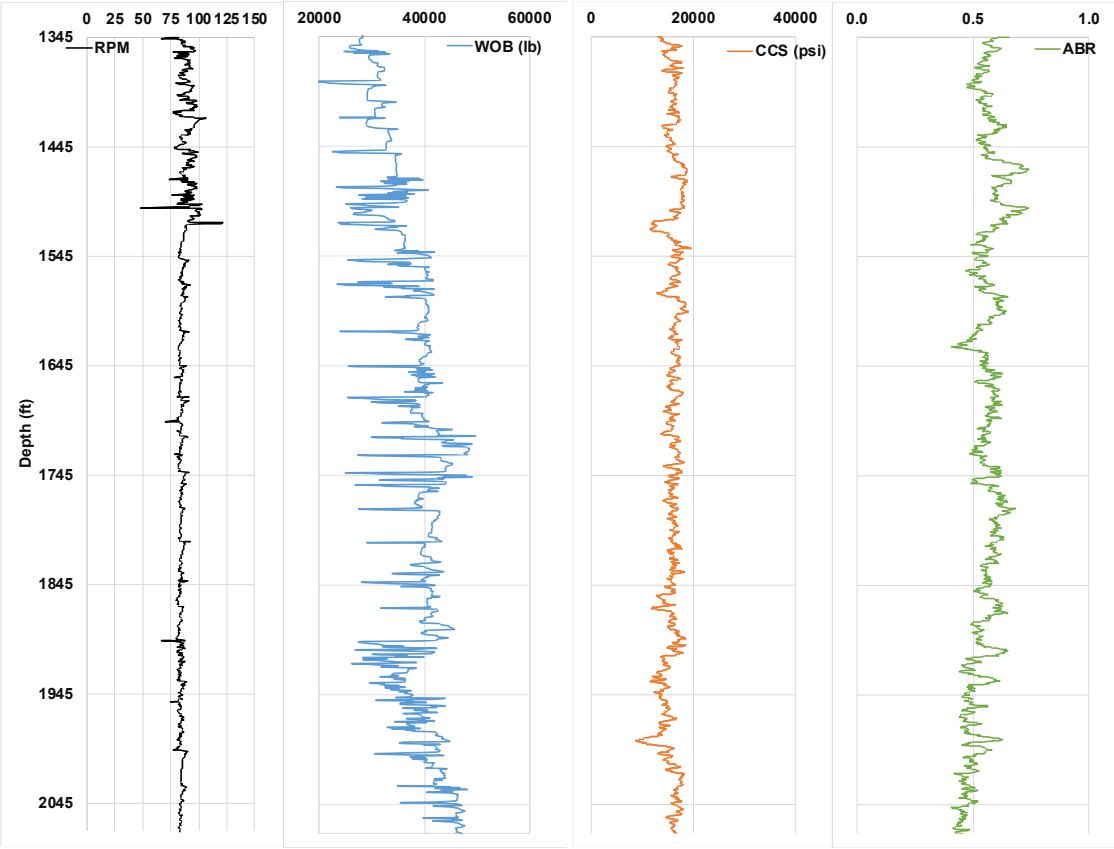

Figure 24: CM Bit #1- time and depth based data match

The final product of the 13 time-based files and the single depth-based files, is a single matched data set that will be used throughout the remainder of this study. All data represented by the file match can be seen side by side in Figure 24. Along with matching all data from CM bit #1 the same procedures were completed on the 11 files for CM bit # 2 and the final results can be seen in later chapters.

CHAPTER IV

RESULTS

4.1 Wear Model Calibration

In order to fully develop a real-time wear model two steps needed to occur. First, was deciding on a model to use for all occasions moving forward. The model selected was that of Motahhari et al. (2010) which was discussed earlier in the section 2.1.

$$\Delta V = C_a \sum_{i=d_{in}}^{d_{out}} \left(\frac{WOB_i}{1000n}\right)^{C_1} * RPM_i^{C_2} * \frac{S_i}{1000} * Abr_i \qquad \text{Eq. 4.1}$$

The reason for selecting this model is because it uses common drilling parameters, WOB and RPM, and rock properties that can be measured while drilling, rock strength (S_i) and abrasiveness (Abr_i). Aside from being a function of commonly available drilling parameters and rock properties, this model also calculates an actual volumetric value instead of a wear function similar to Equation 2.11. Even though the Motahhari model is simple in the fact that it only uses readily available parameters, the model is not useful if C_a, C_1 and C_2 are not calibrated. Using the single cutter data, this model was able to be calibrated because of the variation of WOB and

RPM amongst that data. Five separate cutters from the single cutter testing were selected. All five cutters selected had a wear volume remaining within the PDC layer and had the same test duration. After selecting the five cutters with constant material wear and same time but varying WOB and RPM, as seen in the table below, the model has enough data points to be calibrated.

Cutter #	Time (min)	WOB	RPM	Worn Volume (in^3)
New	-	0	0	0
2	60	270	75	$1.42x10^{-5}$
6	60	296	125	$2.40x10^{-5}$
10	60	501	75	$1.53x10^{-5}$
13	60	705	125	$3.01x10^{-5}$
16	60	791	75	$1.87x10^{-5}$

Table 2: Selected cutters for wear model

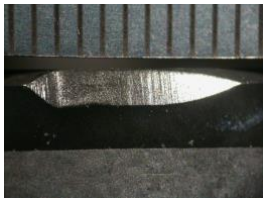

Cutter 2

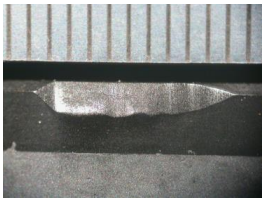

Cutter 6

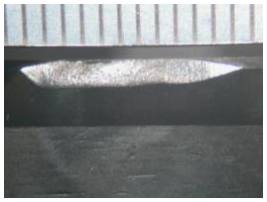

Cutter 10

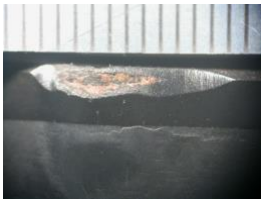

Cutter 13

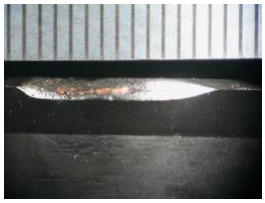

Cutter 16

Figure 25: Photos of the 5 cutters selected for wear model calibration

In order to calibrate the PDC wear model, the abrasiveness and rock strength were eliminated from Equation 4.1, seen in Equation 4.2 below.

$$\Delta V = C_a \sum_{i=d_{in}}^{d_{out}} \left(\frac{WOB_i}{1000n}\right)^{C_1} * RPM_i^{C_2} \quad \text{Eq.4.2}$$

The theory behind eliminating abrasiveness and rock strength is based on the assumption that each cutter tested is contacting each different part of the test rock for the same amount of time. All cutters are contacting the Yellow Torrey Buff Sandstone, Red Sandstone and Texas Pink Granite for approximately one third of the test or 20 minutes each. It is noted that each test was performed on the same rock pie. Based on this the assumption was made that the abrasiveness and rock strength were equal across all tests.

The updated wear equation was loaded into the DEA solver resulting in C_a=2.76x10-7, C_1=0.267 and C_2=0.991. As seen below in Figure 26, when the initial parameters were placed into the calibrated model to calculate the worn volumes, the results were within 1% of the raw worn volume values.

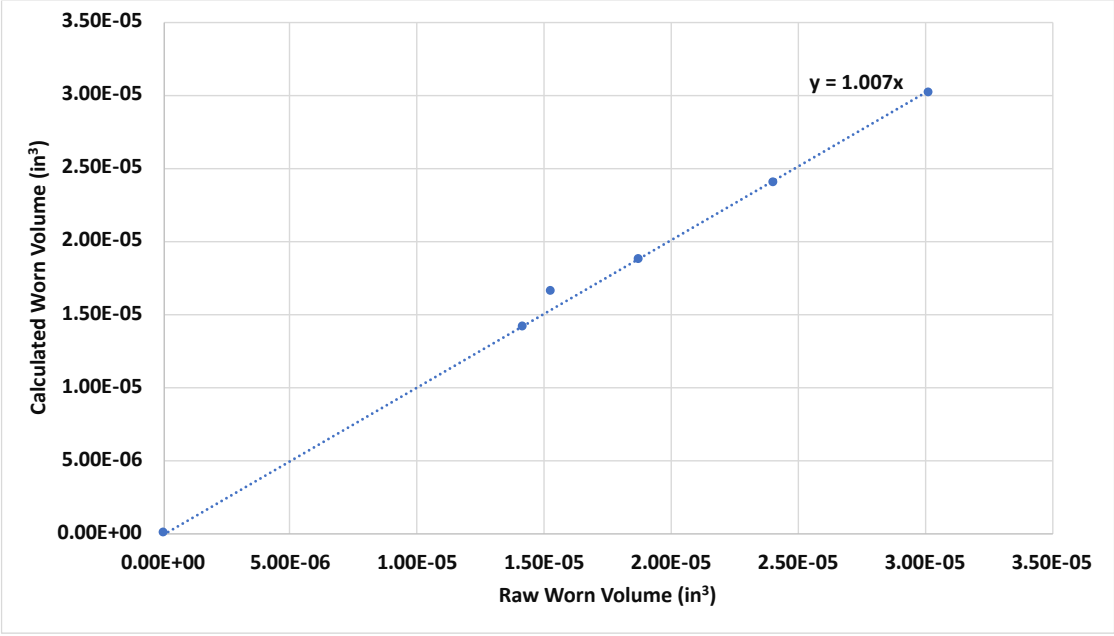

Figure 26: Volumetric calculation verification

Figures 27 and 28, display the accuracy and how it responds to the two operating parameters, WOB and RPM.

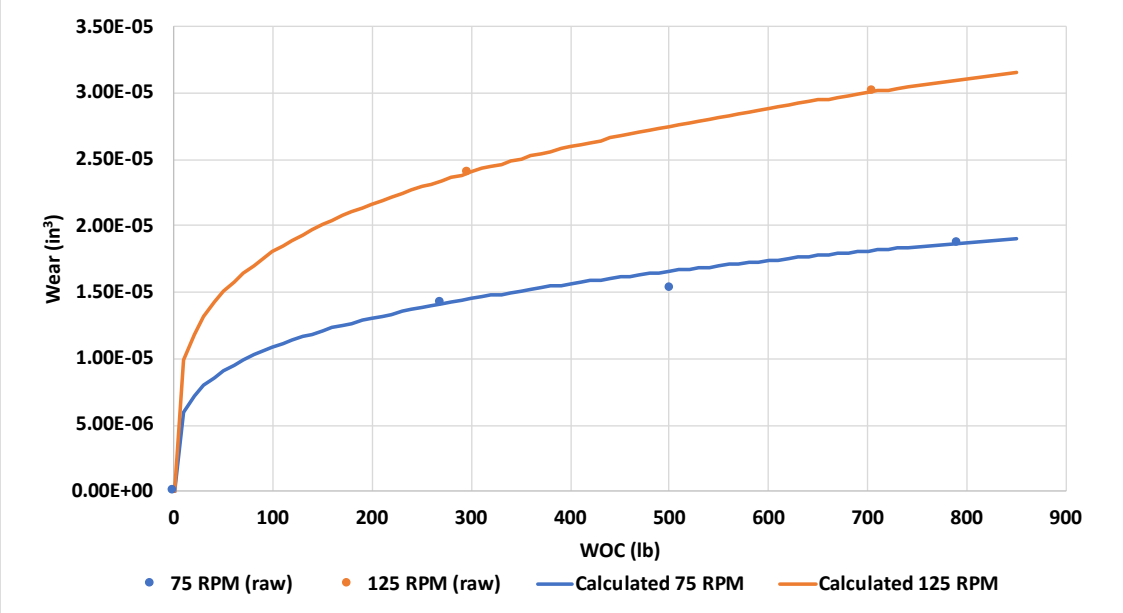

Figure 27: Model calculations for change in WOB

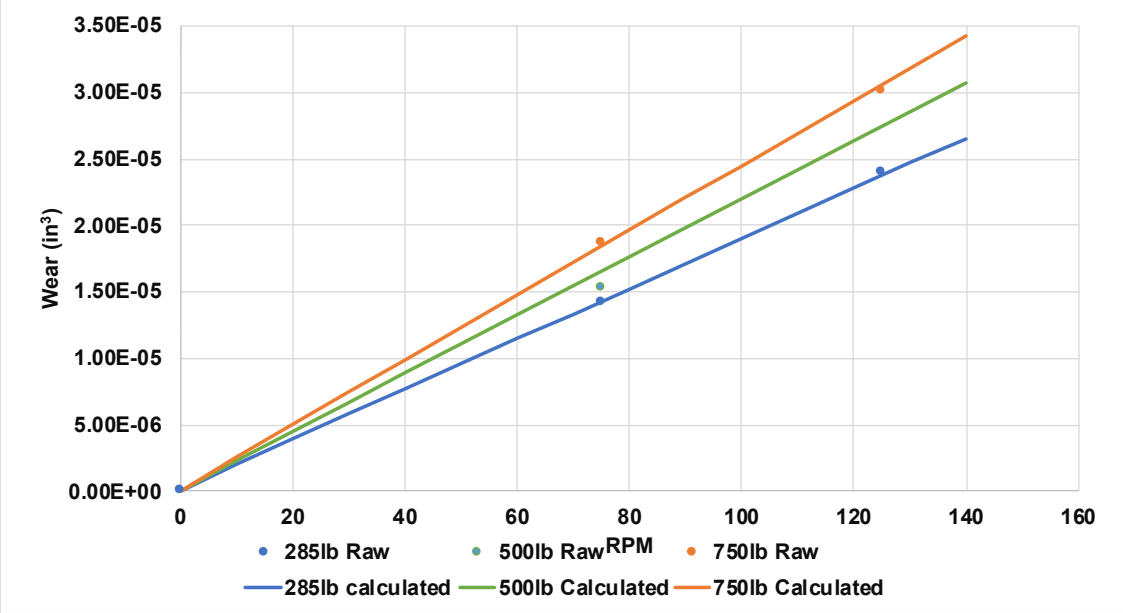

Figure 28: Model calculations for change in RPM

Within the wear model, C_a is considered a bit constant, which will vary from bit to bit. C_1 and C_2 will remain constant throughout all subsequent uses throughout this study and in actual applications. The resulting equation for the calibrated wear model is

$$\Delta V = C_a \sum_{i=d_{in}}^{d_{out}} \left(\frac{WOB_i}{1000n}\right)^{0.262} * RPM_i^{991} * \frac{S_i}{1000} * Abr_i \qquad \text{Eq. 4.3}$$

4.2 Accelerated Wear

The model in section 4.1 was solely calibrated based on PDC wear. The single cutter tests provided by a third party selected to calibrate the model had yet to reach the carbide layer and that is based on accelerated wear that is seen when the carbide layer is reached. As seen in Figure 29, the PDC wear rate remains fairly constant across the eleven tests that only experienced wear within the PDC layer.

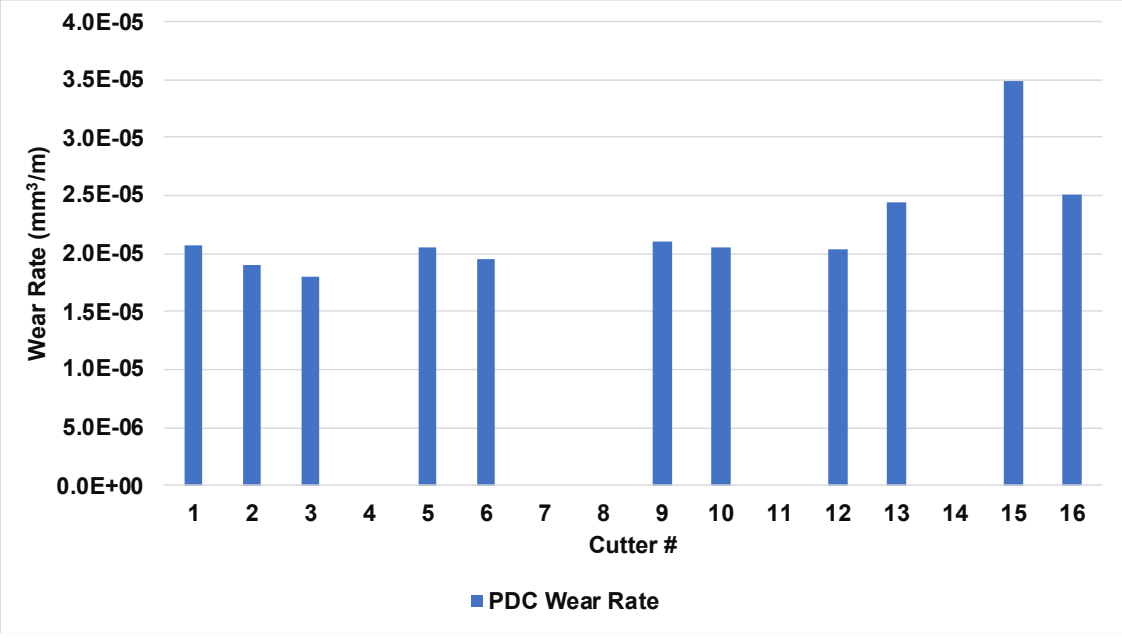

Figure 29: Cutter wear rates before carbide layer is reached

When the carbide wear is introduced into the picture, a drastic increase is seen in the wear rate. Figure 30 shows all 16 cutter wear rates plotted against each other. The average wear rate for the PDC wear only is 2.22×10^{-5} mm^3/m and the average combined wear rate is 5.37×10^{-4} mm^3/m or 24 times greater than that of the PDC alone.

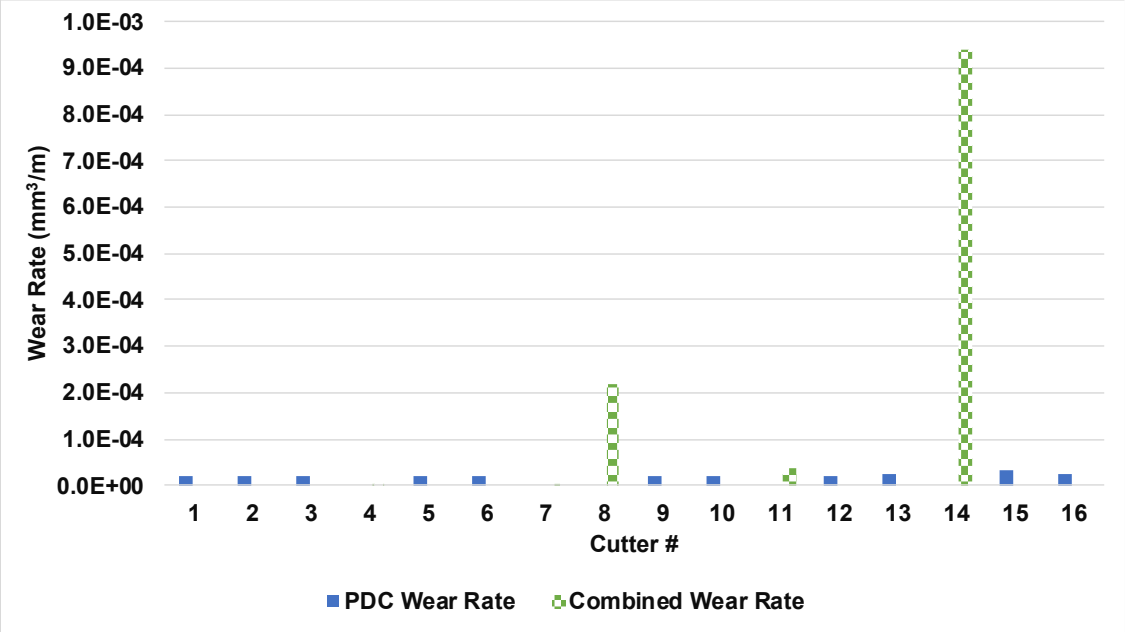

Figure 30: Cutter wear rates PDC only and combined

Looking closely at cutters 5-8, Figure 31, it can be seen that cutter wear continually increases once the carbide layer is reached. This coincides with what was reported by Li et al (2005) about tungsten carbide wear rate rapidly increasing as cutting progresses. It can be seen in Figure 28, that the wear rate of the PDC decreases as the cutting progresses; cutters 1-3, 5-6, 9-10 and 15-16. Leaving cutters 12-13 the only group that PDC wear rate increased as the cutting distance progressed.

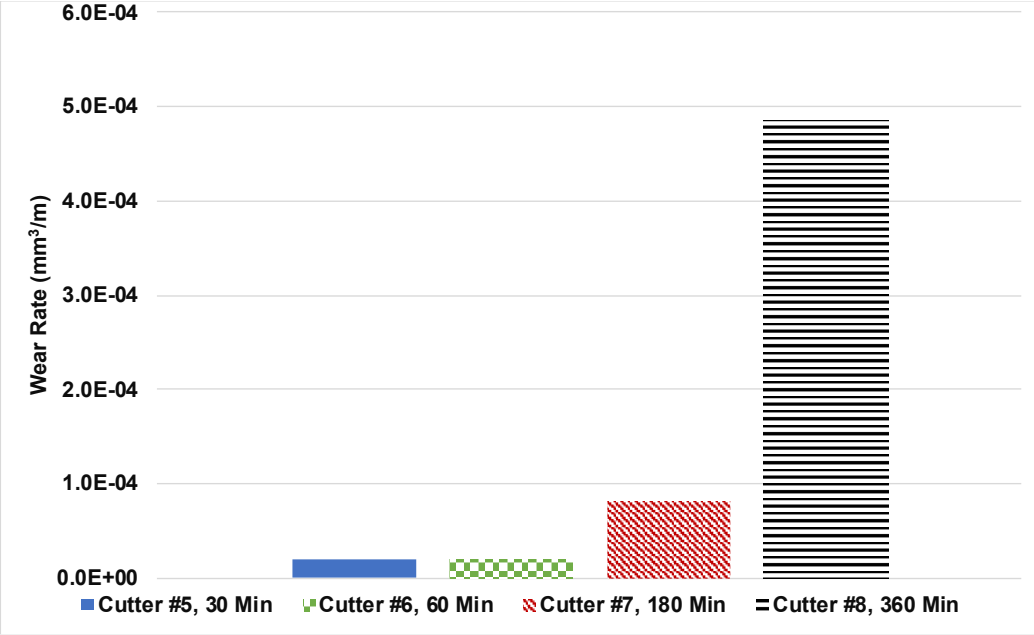

Figure 31: Varying cutter wear with equal operating parameters
(WOB: 296 lb and RPM: 125)

There is only one case where there is a group of consecutive tests with combined PDC and carbide wear. Pairing these results with that reported by Li et al. (2005) leads to the point that PDC wear models can be based solely on PDC wear rates if accumulating only for the PDC lost.

4.3 Wearflat Temperature

Accelerated bit wear can also be seen when the PDC critical temperature is reached. By keeping the PDC wearflat temperature below this, the wear rate can remain stable and allow for longer bit runs due to maximizing bit life. The PDC wearflat temperature is a function of WOB and RPM, therefore decreasing these parameters can help in avoiding the critical temperature. In order to implement a real-time wearflat temperature measurement, the Glowka et al. wearflat temperature model needed to be verified.

$$\bar{T}_w = T_{fl} + \frac{KFvf}{A_w\left[1 + \frac{3\pi}{4}K_{hf}f\left(\frac{v}{\eta L_w}\right)^{\frac{1}{2}}\right]} \qquad \text{Eq. 4.4}$$

Once again, the data received from the single cutter testing were used for this verification. Four cutters (2, 3, 6 and7) were selected based on the fact that they had two separate tests that were within a stable temperature range at the end of the test. The four cutters were grouped as 2-3 and 6-7. The cutters that were grouped had the same operating conditions but were tested for different durations. Cutters 2 and 6 were both 60-minute tests, while cutters 3 and 7 were 180-minute test. The following table shows the values for the calculated temperature compared to the recorded temperature.

Parameters	Wear Flat (in^2)	Calculated Temp. (°F)	Measured Temp. (°F)
Glowka (Stable)	3.10E-02	668	662
#2 (Unstable)	1.35E-02	989	527
#3 (Stable)	2.46E-02	666	617
#6 (Unstable)	1.45E-02	1309	518
#7 (Stable)	4.66E-02	648	673

Table 3: Wearflat temperature verification

In table 3, it is seen that cutters #2 and #6 were not within an acceptable range of the recorded temperature during testing. The reason that the calculated value did not coincide with the recorded data is due to the small wearflat area. When the wearflat area is too small it drives the temperature equation near its upper limits. Due to this, the temperature calculation is not accurate until a substantial wearflat area has been achieved. Again, referring to table 3, cutter #3 temperature is overestimated and cutter #7 is slightly underestimated, this gives reason that a wearflat area near 0.025 in_2 should be large enough to get an accurate estimate for wearflat temperatures while drilling.

4.4 Field Case Validation

Field case data were used from a well in Chocolate Mountain (CM) gunnery range field and bit wear were matched to verify the use of the wear model from section 4.1. The verification was performed on two separate bit runs. Bit #1 drilled from 1345 to 2070 ft and Bit #2 drilled from 2070 to 2643 ft. Bit #1 came with a complete data set but Bit #2 was missing data from depths of 2420 to 2520 ft.

4.4.1 Bit #1

Bit #1 was an 8-1/2 inch type DRS813M-B21 commercial bit received from an NOV warehouse in Bakersfield, CA. Bit #1 was equipped with arrestors that keep the bit from achieving a depth of cut which is too large. The arrestors can limit the ROP but are installed to prevent cutter damage by mitigating excess WOB. The bit after drilling can be seen in Figure 33. It was reported that the bit was carefully examined after being pulled and the bit had endured minimal damage and would have been capable of drilling further.

Figure 32: Bit #1 before drilling

Figure 33: Bit #1 after drilling

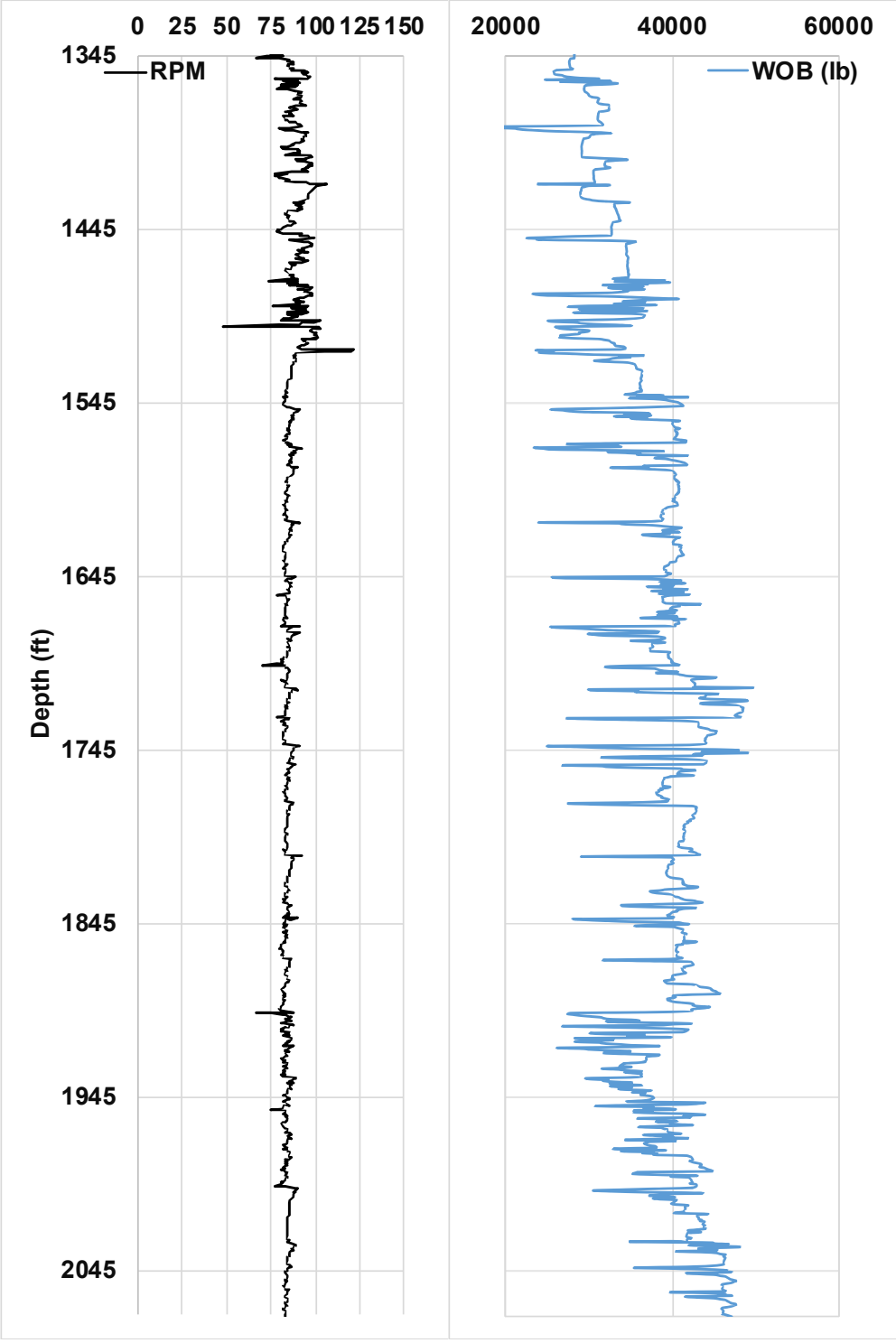

Figure 34: Operating parameters from Chocolate Mountain Bit #1

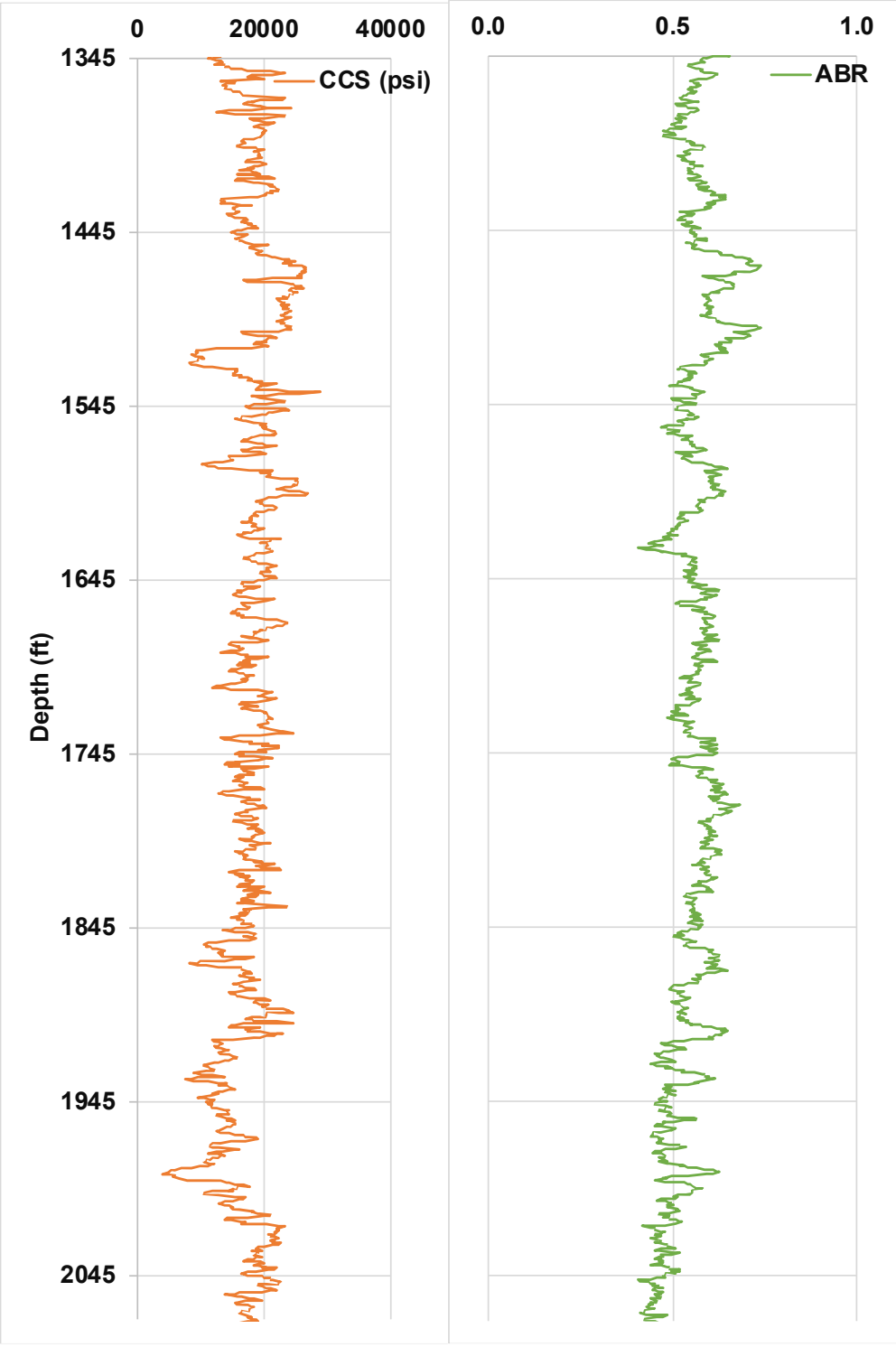

Figure 35: Rock properties from Chocolate Mountain Bit #1

Above, in Figures 34 and 35, are the parameters that will be used in the wear model. Applying RPM, WOB, CCS and abrasiveness from the field to the model discussed in section 4.1, it is possible to calculate the bit wear. Using Equation 4.3 with a bit constant of $Ca=6.77x10^{-12}$, paired with the field data above, a real-time bit grade or worn volume can be calculated as seen in Figure 36. At the time Bit #1 stopped rotating, BG=1.8 and the total volume removed from a single cutter averaged 0.008 in^3.

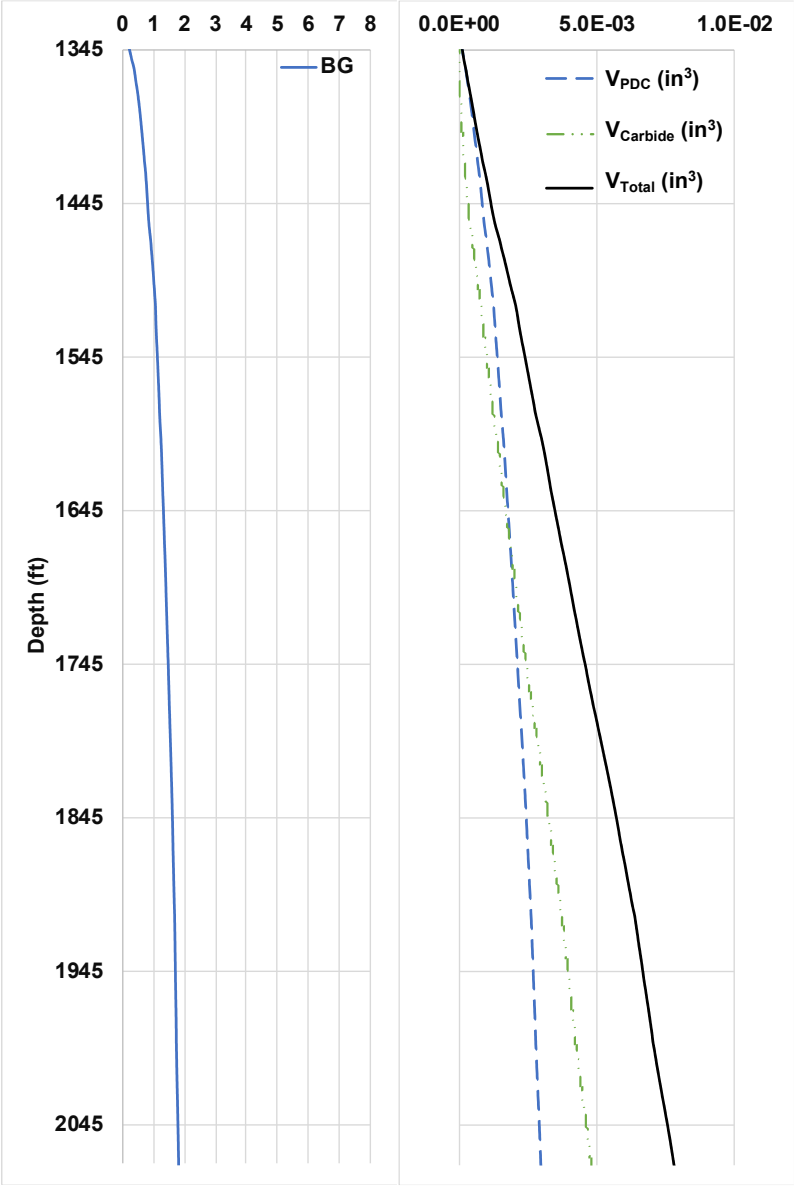

Figure 36: Example of bit #1 wear while drilling

Aside from accurately estimating BG during the Bit #1 run, temperature calculations can simultaneously be done to ensure that the wearflat temperature remains under the material critical temperature. Using the constants that were applied for fluid drilling outlined in the Glowka paper, the same operational parameters can be applied from above to calculate wearflat and PDC temperatures as seen in Figure 37. The temperatures remained well below 662 ºF (350 ºC), reported as the critical temperature by Glowka, but it can be noted that the PDC temperature quickly responds to the increase in WOB.

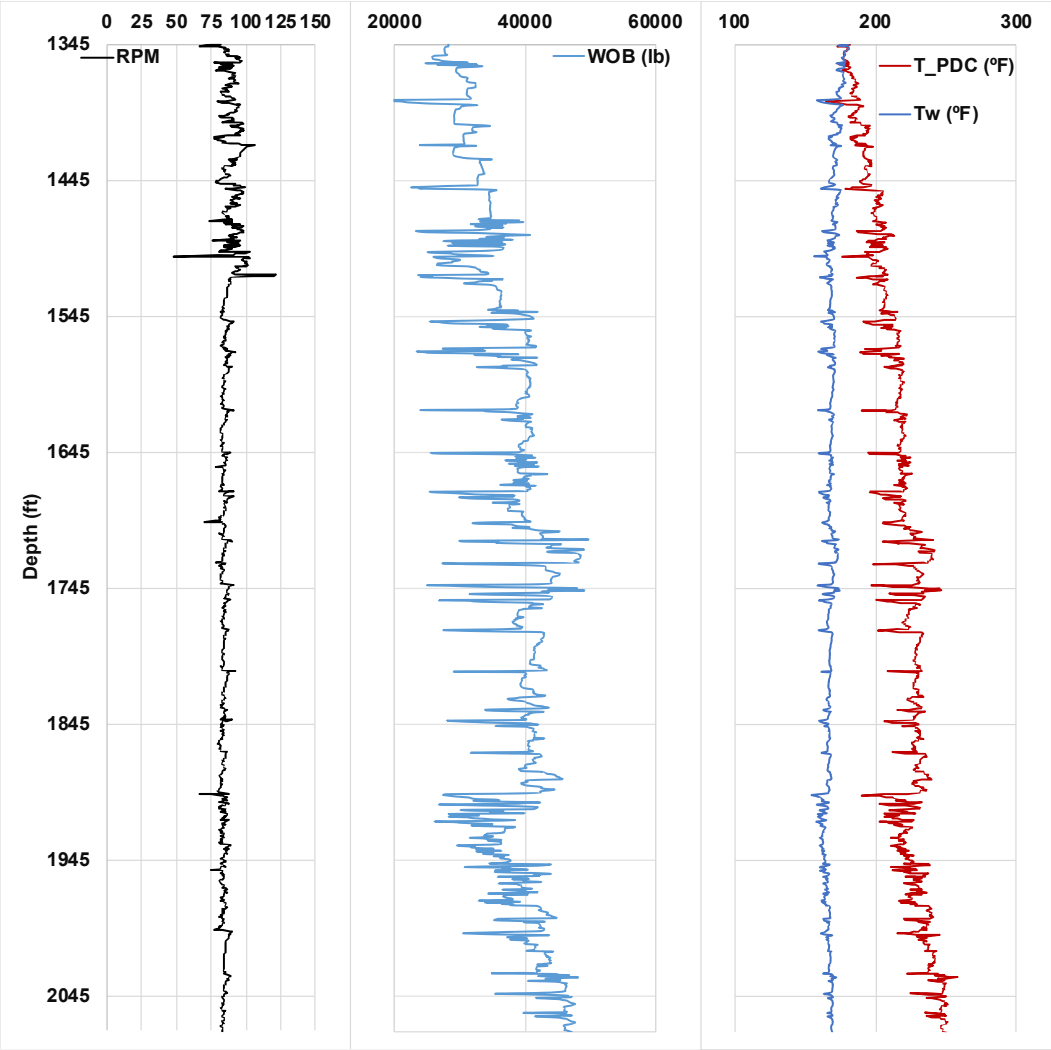

Figure 37: Operating parameters and example of bit #1 wear flat and PDC temperature while drilling

4.4.2 Bit #2

Bit #2 was an 8-1/2 inch NOV type RH DSR713M-B21 PDC Bit with seven blades and did not have arrestors like Bit #1. Since bit #2 does not have arrestors, it was a more aggressive bit. After pulling the bit, a visual inspection verified that three cutters on the inside two rows of the bit were missing. It was noted that the cause of the missing cutters is most likely due to the excessive dynamic/impact loading due to running the bit close to the torque stall point of the rig and having to restart the bit from frequent torque stalls and drill-offs. Aside from the three missing cutters, it was reported that cutter wear was minimal but is greater than that of bit #1.

Figure 38: Bit #2 before drilling

Figure 39: Bit #2 after drilling

As stated earlier, Bit #2 was missing RPM and WOB data for roughly 100 ft of the drilling but the same process was performed on bit #2 as was done on bit #1. Figures 40 and 41 are a representation of the Bit #2 operating parameters and the rock properties associated. These four parameters underwent the same QC procedures that were performed on Bit #1 in section 3.4.2.

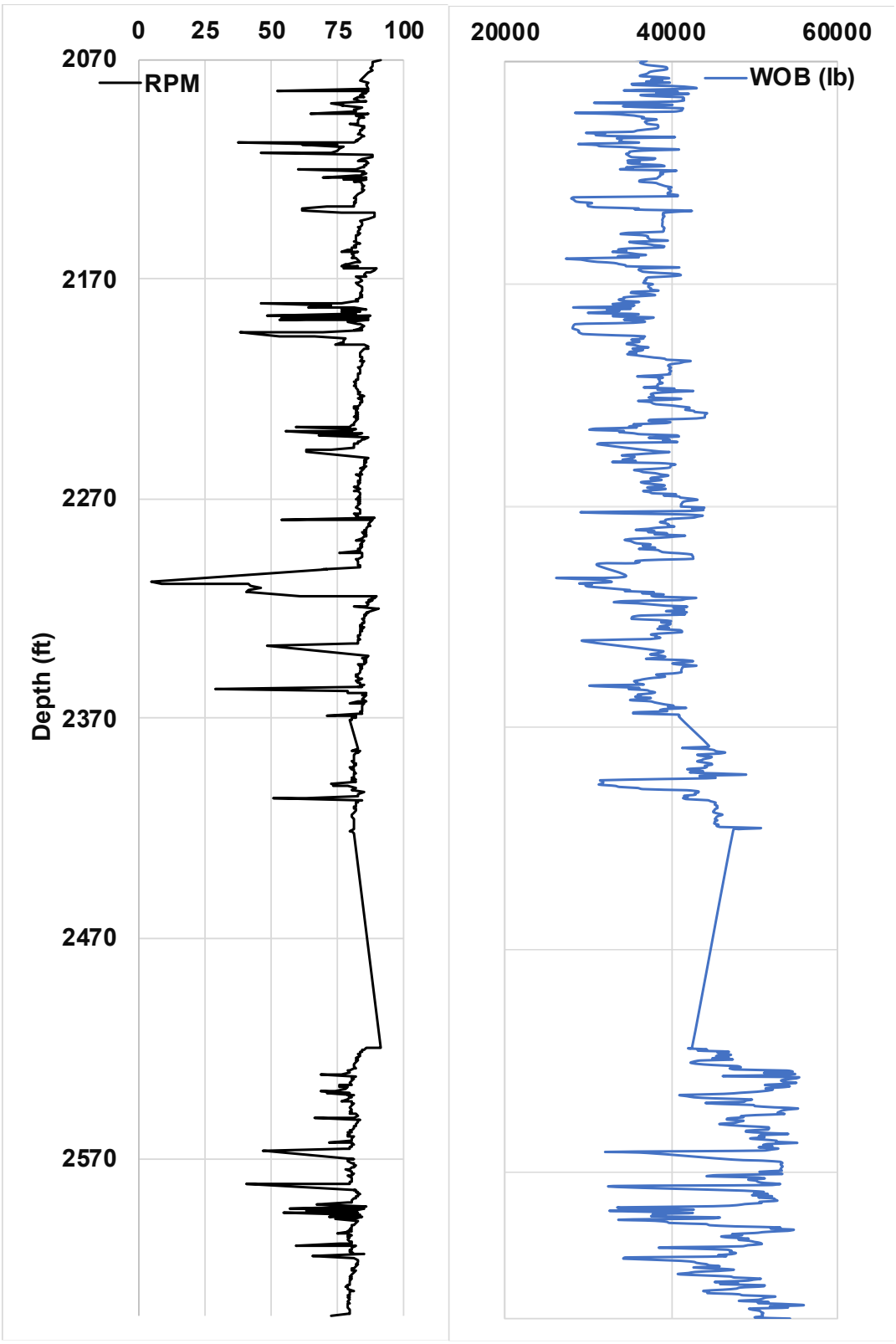

Figure 40: Operating parameters Chocolate Mountain Bit #2

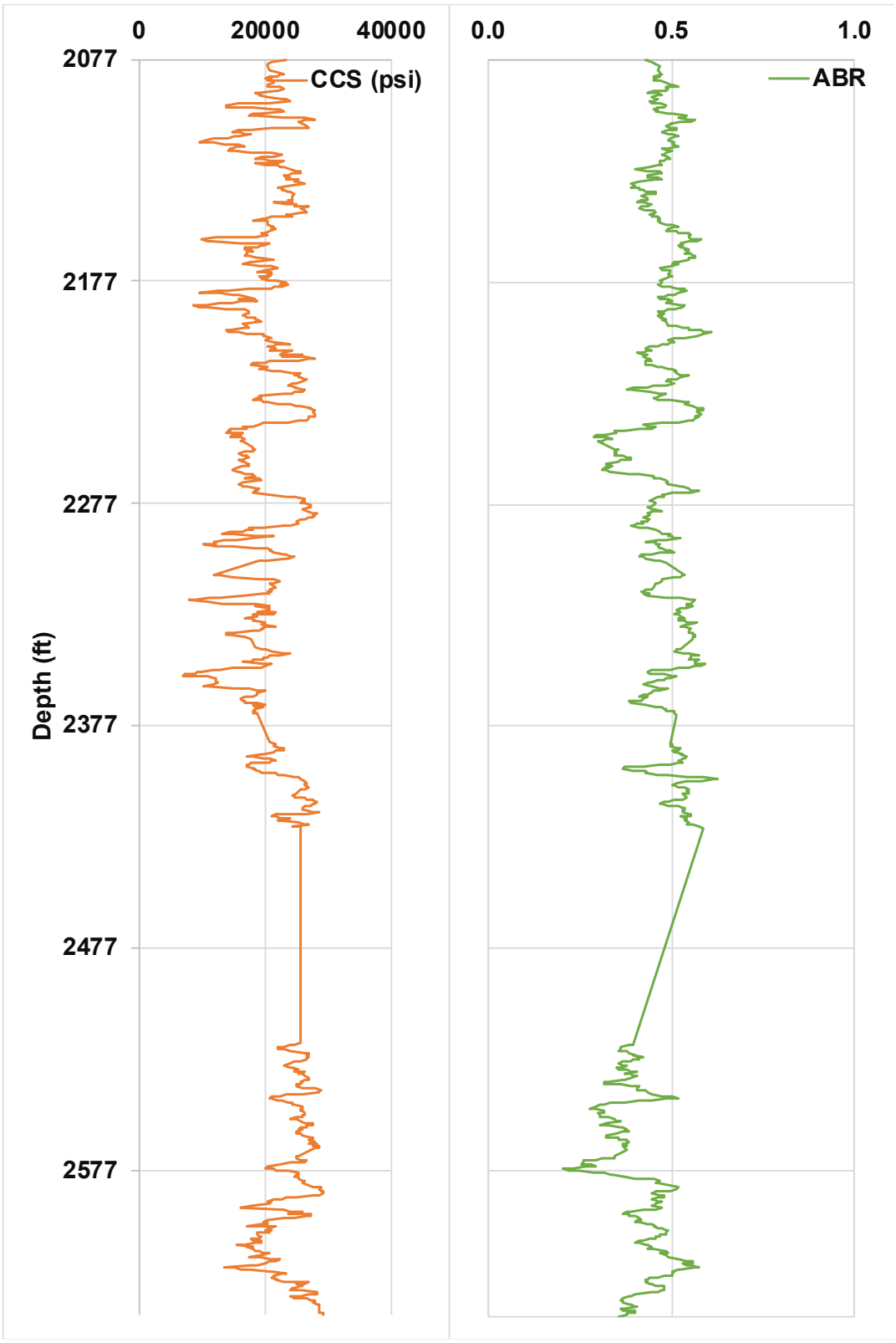

Figure 41: Rock properties from Chocolate Mountain Bit #2

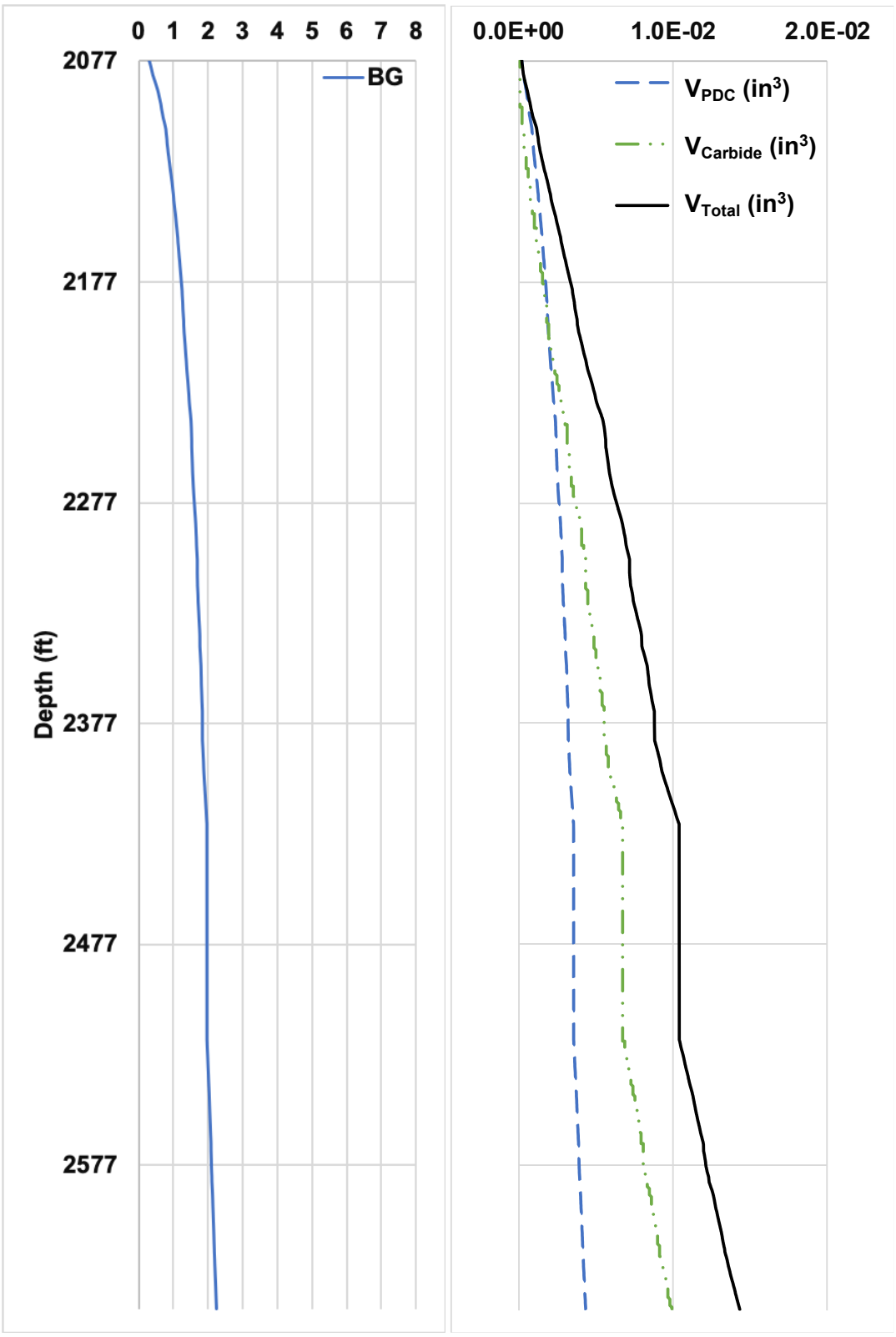

Figure 42: Example of bit #2 wear while drilling

Bit #2 experienced more cutter wear than that of Bit #1. Due to the fact that Bit #2 did not have arrestors, to limit the WOB seen by the cutters, and the loss of three cutters, a C_a value of $1.89x10^{-11}$ was used. It should be noted, if a full data set was available for Bit #2, the value for C_a would be lower. The fact that 100 ft of drilling data is missing inflates the bit constant to account for the volume lost in that section. At the time Bit #2 stopped rotating, bit grade was 2.25 and the total volume removed from a single cutter averaged 0.014 in^3.

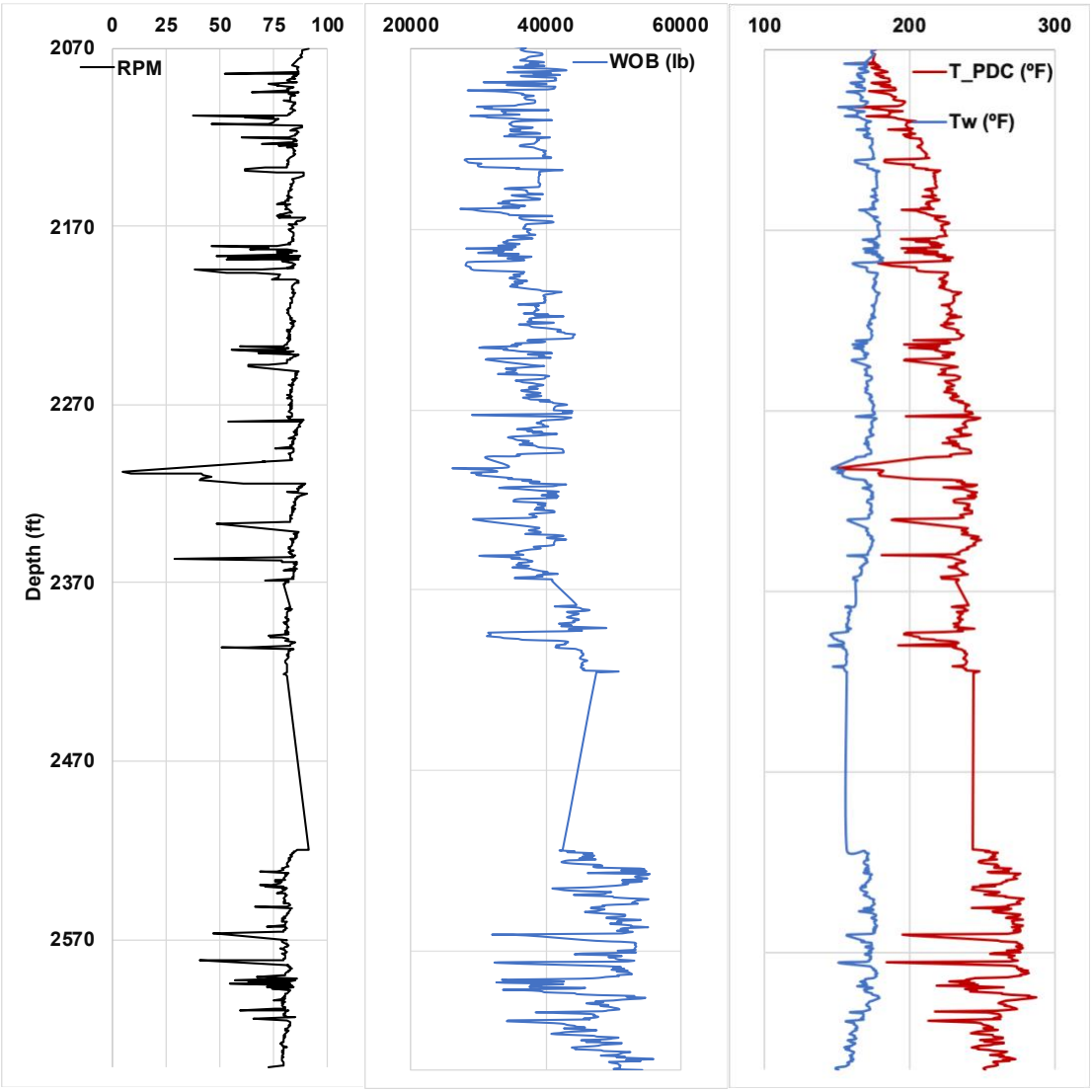

Figure 43: Operating parameters and example of bit #2 wear flat and PDC temperature while drilling

4.5 Field Case Comparison

After all the calculations were completed for both bit runs, a comparison of the data was done. In Table 4, the average operating parameters and max volume/temperatures can be seen for each bit.

Parameters		Bit #1	Bit #2
	Feet Drilled	725	573
	C_a	$6.77x10^{12}$	$1.89x10^{11}$
Avg.	**WOB (lb)**	37690	40801
	RPM	86	80
	CCS (psi)	15896	21200
	ABR	0.55	0.46
Max	**BG**	1.8	2.3
	V_{Total} (in3)	0.008	0.014
	$V_{Carbide}$ (in3)	0.005	0.010
	V_{PDC} (in3)	0.003	0.004
	T_w (°F)	196	192
	T_{PDC} (°F)	257	287

Table 4: Bit #1 and #2 comparison

When looking at the data side by side we can see that Bit #2 experienced almost two times the wear while drilling roughly 150 ft less than Bit #1. The accelerated wear was caused by multiple factors. First, WOB and CCS is much higher for Bit #2 which would result in faster wear. Second, along with the increase in WOB, Bit #2 did not have arrestors like Bit #1, which would ultimately limit the WOB seen by Bit #1. Last, carbide wear is doubled from Bit #1 to Bit #2, while the PDC wear increased by only 33%.

CHAPTER V

Conclusion

5.1 Summary

This project has been done in conjunction with other individuals from Oklahoma State University, University of Oklahoma and Sandia National Laboratory in efforts to develop a real time drilling advisory model. The efforts of this research were achieved through single cutter PDC testing, PDC wear modeling and field testing. Single cutter testing, completed by a third party, was performed on a rock pie consisting of three different rock strengths. Based on the data received from testing it was concluded that PDC wear rates remained constant with increased force (WOB) and sliding distance (rotating time), while carbide wear continually increased. Based on these findings, a PDC wear model has been developed using detailed cutter geometry. The PDC wear model can predict wear while drilling, based on drilling parameters and rock properties. With the available details from the cutter geometry and known cutter wear, an accurate model for the cutter wearflat temperature has also been achieved. The models established from this analysis were then verified using field data from two separate bit runs. By accurately accounting for bit wear and having a real time prediction for wearflat temperature, a parameter map can now be implemented that will give an optimum range for WOB and RPM to achieve the greatest ROP for the next foot to be drilled.

5.2 Future Work

While the conclusion of this research has achieved the goals that were set out in the inception of this project, there are areas that benefit from further work. To further expand on the work that has been completed, accumulating bit constants for common bits used in the industry would accelerate the implementation of this real time drilling model. By creating a database that stores the bit constant, Ca, would eliminate the need for a new user to calibrate Ca for bits they are using.

Along with a data base for bit constants, information regarding cutter qualities should be collected. Through this research, the cutters studied were all of the same quality but cutter quality can vary from manufacturer to manufacturer and also for different types of cutters. Further information on individual cutter quality would be beneficial to the implementation of this drilling model.

Last, further work on the different wear rates of PDC and Tungsten Carbide should be completed. A definite increase in total wear rate was seen when the Carbide layer was reached, but testing on PDC only and Carbide only in the same facility would lend further detail to this subject matter and possible aid to a more accurate representation of cutter wear.

REFERENCES

Appl, F., Wilson, C. C., & Lakshman, I. (1991). Measurement of Forces, Temperatures, And Wear of PDC Cutters in Rock Cutting. Society of Petroleum Engineers. doi: 10.1016/0043-1648(93)90386-Z

Atashnezhad, A. (2019). Incorporating the Interfacial Friction Angle Concept into the PCD Single Cutter and Full Bit Modeling. Oklahoma State University, PhD dissertation.

Geoffroy, H., Minh, D. N., Bergues, J., & Putot, C. (1998, January 1). Frictional Contact on Cutters Wear Flat and Evaluation of Drilling Parameters of a PDC Bit. Society of Petroleum Engineers. doi:10.2118/47323-MS

Glowka, D A. Development of a method for predicting the performance and wear of PDC (polycrystalline diamond compact) drill bits. United States: N. p., 1987. Web. doi:10.2172/5591640.

Glowka, D., & Stone, C. (1986, June). Effects of Thermal and Mechanical Loading on PDC Bit Life. SPE Drilling Engineering, 1(03). doi:https://doi.org/10.2118/13257-PA

Kuru, E., & Wojtanowsicz, A. (1988). A Method for Detecting In-Situ PDC Bit Dull and Lithology Change. IADC/SPE Drilling Conference (pp. 137-152). Dallas: Society of Petroleum Engineers.

Liu, Z., Marland, C., Li, D., & Samuel, R. (2014, May 21). An Analytical Model Coupled with Data Analytics to Estimate PDC Bit Wear. Society of Petroleum Engineers. doi:10.2118/169451-MS

Li, X.S., Boland, J.N. The Wear Characteristics of Superhard Composite Materials in Abrasive Cutting Operations, Wear, Volume 259, Issues 7–12, 2005, Pages 1128-1136, ISSN 0043-1648

Motahhari, H. R., Hareland, G., & James, J. A. (2010). Improved Drilling Efficiency Technique Using Integrated PDM and PDC Bit Parameters. Society of Petroleum Engineers. doi:10.2118/141651-PA

Onyia, E. C. (1988, January 1). Relationships Between Formation Strength, Drilling Strength, and Electric Log Properties. Society of Petroleum Engineers. doi:10.2118/18166-MS

Ortega, A., & Glowka, D. A. (1984, April). Frictional Heating and Convective Cooling of Polycrystalline Diamond Drag Tools During Rock Cutting. Society of Petroleum Engineers Journal, 24(02)

Rahmani, R. (2019, March 4). Rock Customized Shaped Cutters Improve Rock Cutting Efficiency. Society of Petroleum Engineers. doi:10.2118/194148-MS

Raymond, David & Knudsen, S. & Blankenship, D. & Bjornstad, S. & Barbour, J. & Schen, A.. (2012). PDC bits outperform conventional bit in geothermal drilling project. Transactions - Geothermal Resources Council. 36. 307-315

Warren, T., & Sinor, A. (1986). Drag Bit Performance Modeling. Society of Petroleum Engineers. doi:10.2118/15618-MS

Way, Herbert W. L. “The Minerals of Sze-Chuan, China.” The Mining Magazine, 1916, pp. 20–23.

Winters, W. J., Warren, T. M., & Onyia, E. C. (1987, January 1). Roller Bit Model With Rock Ductility and Cone Offset. Society of Petroleum Engineers. doi:10.2118/16696-MS

Wong, A., Bell, A., Williams, M., Isnor, S., & Herman, J. J. (2016, October 19). New Material Technologies Reduce PDC Drill Bit Body and Cutter Erosion in Heavy Oil Drilling Environments. Society of Petroleum Engineers. doi:10.2118/181196-MS

APPENDICES

A.1 Cutter Worn Volume Calculations

The following work was completed by Atashnezhad (2019) and is here only for support to this study. The goal of this section is to find the volume of the worn out section of a cutter. The worn out section for a cutter is seen (assigned number 1) in the Figure A1.

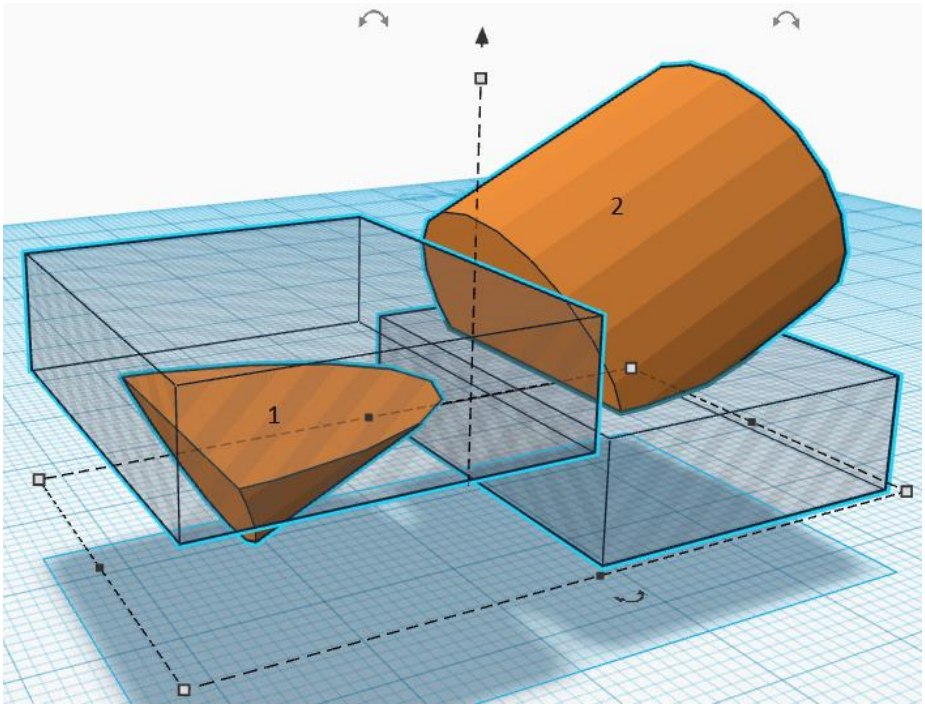

Figure A1. 3D schematic of a blunt cutter (assigned number 2) and the worn section (assigned number 1)

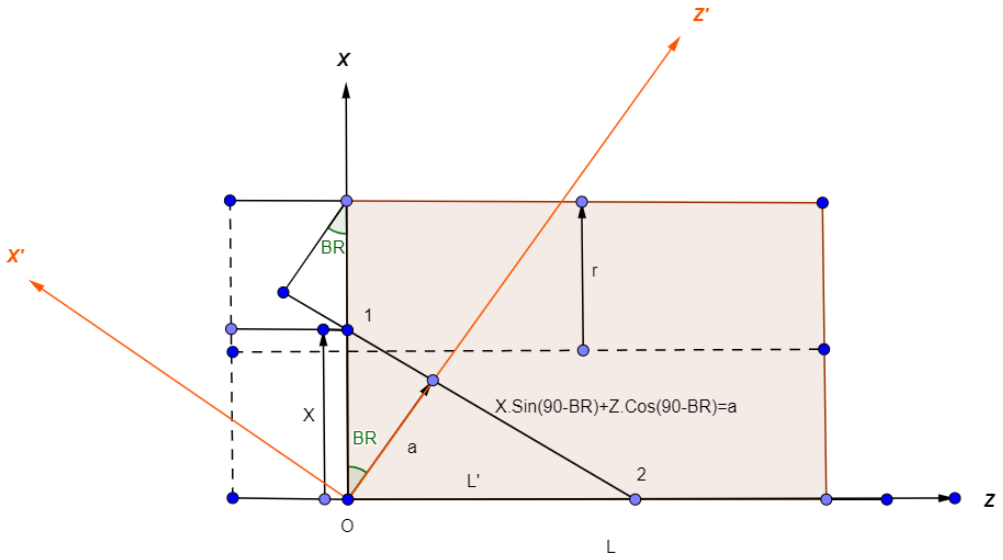

Figure A2. A schematic of cutter side view

Figure A2 shows a cylinder (cutter) laid down on Z axis. The face of cylinder is on the X –Y and is shown in the Figure A3. The Y axis is perpendicular to X and Z plane and it comes out of X-Z origin (point O). In the Figure A2, the line that connect point 1 to point 2 is a 2D representation of a plane in the X'-Z' coordinate. In Figure A2, the L is the length of cylinder. The L' is the length of line between O and point 2. The goal is to calculate the volume of worn wedge (assigned 1 in Figure A1) that is seen as a 2D triangle between point O and points 1 and 2 in Figure A2. The circle segment area can be calculated using Equation A.1.

$$A_{segment} = \left(\frac{D_c}{2}\right)^2 . Cos^{-1}\left(\frac{\frac{D_c}{2} - X}{\frac{D_c}{2}}\right) - \left(\frac{D_c}{2} - X\right) . \sqrt{2.\left(\frac{D_c}{2}\right).X - (X)^2} \ldots\ldots\ldots \text{Eq. A. 1}$$

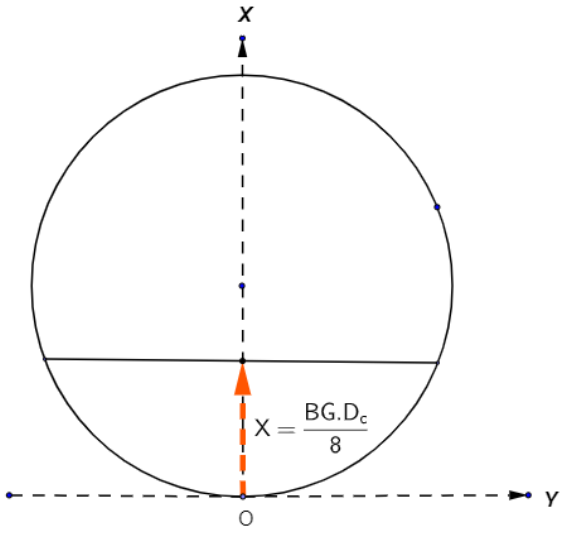

Figure A3. Cutter front face on X-Y coordinate (front side view)

The area of circle segment in Figure A3, is function of X using Equation A.1. The variable X in the circle, then can be written as a function of Z (see Equation A.7). The cutter worn volume can be found by taking an integral of circle segment area (Equation A.1) and between Z=0 and Z=b (point 1 and 2 in the Figure A.2). For above integral the lower boundary is calculated by X=0 in plane Equation (Equation A.2). The Equation A.2, is achieved by replacing θ with the 90-BR.

$$a = X.Sin(90 - BR) + Z.Cos(90 - BR) \ldots\ldots\ldots \text{Eq. A. 2}$$

The L' is calculated using Equation A.3 (see Figure A.2).

$$L' = \frac{a}{Cos(90 - BR)} \ldots\ldots\ldots \text{Eq. A. 3}$$

In the Equation A.3, the a is depth of worn and it is seen in Equation A.4.

$$a = \left(\frac{BG.D_c}{8}\right).Cos(BR) \ldots\ldots\ldots \text{Eq. A. 4}$$

Replacing a from Equation A.4 into Equation A.3 will result in Equation A.5.

$$L' = \frac{\left(\frac{BG.D_c}{8}\right).Cos(BR)}{Cos(90 - BR)} = \frac{\left(\frac{BG.D_c}{8}\right).Cos(BR)}{Sin(BR)} = Cot(BR).\left(\frac{BG.D_c}{8}\right) \text{ …… Eq. A. 5}$$

The X in Equation A.1 is provided in the following.

$$X = f(z) \text{ …… Eq. C. A}$$

Replacing a line equation into Equation C.6 will results in Equation A.7.

$$X = A.Z + B \text{ …… Eq. A. 7}$$

To achieve the coefficients of the line in Equation A.7, two points are needed.

A.1.1 Cutter Worn Volume Calculation (including PDC and STUD)

In this case, the point 2 intersection is less than cylinder length and then

$$Condition: L' < L$$

Intersection points (point 1 and 2 in Figure A.2) are:

$$\begin{pmatrix} intersection\ points \\ point1 = \\ point2 = \end{pmatrix} \begin{pmatrix} X & Z \\ \frac{BG.D_c}{8} & 0 \\ 0 & L' = Cot(BR).\left(\frac{BG.D_c}{8}\right) \end{pmatrix}$$

The A and B are found by taking the above intersection points and Equation A.7 into account (see Equations A.8 and A.9).

$$A = -Tan(BR) \text{ …… Eq. A. 8}$$

$$B = \left(\frac{BG.D_c}{8}\right) \text{ …… Eq. A. 9}$$

Equation A.7 is turned into Equation A.10 using Equation A.8 and A.9.

$$X = -Tan(BR).Z + \left(\frac{BG.D_c}{8}\right) \ldots\ldots\ldots \text{Eq. A. 10}$$

Replacing X from Equation A.10 into Equation A.1 will result in Equation A.11.

$$A_{segment}$$

$$= \left(\frac{D_c}{2}\right)^2 . arccos\left(\frac{\frac{D_c}{2} - \left(-Tan(BR).Z + \left(\frac{BG.D_c}{8}\right)\right)}{\frac{D_c}{2}}\right)$$

$$- \left(\frac{D_c}{2} - (-Tan(BR).Z\right.$$

$$\left. + \left(\frac{BG.D_c}{8}\right)\right). \sqrt{2.\left(\frac{D_c}{2}\right).\left(-Tan(BR).Z + \left(\frac{BG.D_c}{8}\right)\right) - \left(-Tan(BR).Z + \left(\frac{BG.D_c}{8}\right)\right)^2} \ldots\ldots\ldots \text{Eq. A. 11}$$

The cutter worn volume then is calculates by taking an integral from Equation A.11 between boundaries. The integral boundaries are seen in the Equation A.12.

$$\int_0^{Cot(BR).\left(\frac{BG.D_c}{8}\right)} A(Z)dZ \ldots\ldots\ldots \text{Eq. A. 12}$$

The above integral is simplified by separating and defining new variables at the following. The parameters A, D, C and X are defined in Equation A.13.

$$A = \left(\frac{D_c}{2}\right), D = -Tan(BR), C = \left(\frac{BG.D_c}{8}\right), X = Z \ldots\ldots\ldots \text{Eq. A. 13}$$

Replace the A, D, C, and X into the Equation A.13 will results in Equation A.14.

$$\text{I} = \int A^2 \arccos\left(\frac{A - (DX + C)}{A}\right) dX$$

$$- \int (A - (DX + C)).\sqrt{2A(DX + C) - (DX + C)^2}dX \ldots\ldots\ldots \text{Eq. A. 14}$$

The above integral is composed of two separate integrals and it is shown in Equation A.15.

$$\mathrm{I} = \mathrm{I}_1 - \mathrm{I}_2 \ldots\ldots \text{Eq. A. 15}$$

Integral I_1 is seen Equation A.16.

$$\mathrm{I}_1 = \int A^2 \arccos\left(\frac{A - (DX + C)}{A}\right) dX \ldots\ldots \text{Eq. A. 16}$$

The base integral for Equation A.16 is Equation A.17. Therefore, the Equation A.17 is solved at the following.

$$\mathrm{I} = \int \arccos(\theta) d\theta \ldots\ldots \text{Eq. A. 17}$$

Assume u as follow

$$u = \arccos(\theta) \ldots\ldots \text{Eq. A. 18}$$

Take derivation from u in Equation C.18 will results in Equation C.19.

$$du = \frac{-d\theta}{\sqrt{1 - \theta^2}} \ldots\ldots \text{Eq. A. 19}$$

Change the parameters

$$dv = d\theta \rightarrow v = \theta \ldots\ldots \text{Eq. A. 20}$$

Note that: $\int \mathrm{u} dv = \mathrm{uv} - \int \mathrm{v} du$

Rewrite the integral

$$\mathrm{I} = \theta . \arccos(\theta) + \int \frac{\theta . d\theta}{\sqrt{1 - \theta^2}} \ldots\ldots \text{Eq. A. 21}$$

Change the parameters (introduce t) and take derivation

$$t = 1 - \theta^2; dt = -2\theta d\theta \ldots\ldots \text{Eq. A. 22}$$

Replace t into Equation A.22

$$= \theta . \arccos(\theta) - \frac{1}{2}\int \frac{dt}{\sqrt{t}} \ldots\ldots \text{Eq. A. 23}$$

Rewrite the Equation A.23

$$= \theta . \arccos(\theta) - \frac{1}{2}\int t^{\frac{-1}{2}} dt \ldots\ldots \text{Eq. A. 24}$$

Solve and rewrite Equation A.24

$$= \theta . \arccos(\theta) - \frac{1}{2} . \frac{t^{\frac{1}{2}}}{\frac{1}{2}} \ldots\ldots \text{Eq. A. 25}$$

Replace t with θ in Equation A.25 (see Equation A.22).

$$\text{I} = \theta . \arccos(\theta) - \sqrt{1 - \theta^2} \ldots\ldots \text{Eq. A. 26}$$

Therefore the integral (see Equation A.17) solution would be

$$\int \arccos(\theta) d\theta = \theta . \arccos(\theta) - \sqrt{1 - \theta^2} \ldots\ldots \text{Eq. A. 27}$$

Replace the parameters into integral A.17

$$\text{I}_1 = \int A^2 \arccos\left(\frac{A - C}{A} - \frac{DX}{A}\right) dX \ldots\ldots \text{Eq. A. 28}$$

Taking the A^2 out of integral

$$\text{I}_1 = A^2 \int \arccos\left(\frac{A - C}{A} - \frac{DX}{A}\right) dX \ldots\ldots \text{Eq. A. 29}$$

In the Equation A.29, the X coefficient ($\frac{D}{A}$) in arccos comes out of integral and will be multiplied with A^2 as it is shown in the Equation A.30.

The solution of integral I_1 is provided at the following

$$I_1 = \frac{-A^3}{D}\left(\left(\frac{A-(DX+C)}{A}\right).\arccos\left(\frac{A-(DX+C)}{A}\right) - \sqrt{1-(\frac{A-(DX+C)}{A})^2}\right) \dots\dots\text{Eq. A. 30}$$

The second part of the integral I (Equation A.14) is seen in the Equation A.31. The following steps should be taken to solve the Equation A.31.

$$I_2 = \int (A-(DX+C)).\sqrt{2A(DX+C)-(DX+C)^2}dX \dots\dots\text{Eq. A. 31}$$

Change the parameter as it is provided in the Equation C.32

$$y = DX + C \dots\dots\text{Eq. A. 32}$$

Take derivation from Equation C.32

$$dy = DdX \dots\dots\text{Eq. A. 33}$$

Replace the Equations A.32 and A.33 into Equation A.34

$$I_2 = \frac{1}{D}\int (A-y).\sqrt{2Ay-y^2}dy \dots\dots\text{Eq. A. 34}$$

Rewrite the Equation A.34

$$I_2 = \frac{1}{D}\int (A-y).\sqrt{A^2-(y-A)^2}dy \dots\dots\text{Eq. A. 35}$$

Change the parameters using Equation A.36 (similar to Pythagorean Theorem).

$$y - A = A.Sin(\theta) \dots\dots \text{Eq. A. 36}$$

Take derivation from Equation A.36

$$dy = A.Cos(\theta) \dots\dots \text{Eq. A. 37}$$

Replace the Equation A.36 and A.37 into Equation A.35

$$\mathrm{I}_2 = \frac{1}{D}\int A.Sin(\theta).\sqrt{A^2 - A^2.Sin(\theta)^2}\,.A.Cos(\theta)d\theta \dots\dots \text{Eq. A. 38}$$

Taking the constant out of integral

$$\mathrm{I}_2 = \frac{A^3}{D}\int Sin(\theta).Cos^2(\theta)d\theta \dots\dots \text{Eq. A. 39}$$

Change the parameters and define u as following

$$u = Cos(\theta) \dots\dots \text{Eq. A. 40}$$

Take integral from Equation A.40

$$du = -Sin(\theta).d\theta \dots\dots \text{Eq. A. 41}$$

Replace the Equation A.40 and A.41 into Equation A.39

$$= -\frac{A^3}{D}\int u^2 du \dots\dots \text{Eq. A. 42}$$

Solve the Integral in Equation A.42 and replace the u

$$\frac{A^3}{D}.\frac{u^3}{3} = \frac{A^3}{D}.\frac{Cos^3(\theta)}{3} \dots\dots \text{Eq. A. 43}$$

Rewrite and replace the θ (see Equation A.36) as it is provided at the following

$$= -\frac{A^3}{3D}(\sqrt{1 - Sin^2(\theta)})^3 = \frac{A^3}{3D}(\sqrt{1 - (\frac{y - A}{A})^2})^3 \ldots\ldots \text{Eq. A. 44}$$

Replace the y (see Equation A.32) and rewrite the Equation A.44

$$\mathrm{I}_2 = -\frac{A^3}{3D}\left(\sqrt{1 - (\frac{DX + C - A}{A})^2})\right)^3 \ldots\ldots \text{Eq. A. 45}$$

The integral I answer is provided in Equation A.46.

$$\mathrm{I} = \frac{-A^3}{D}\left(\left(\frac{A - (DX + C)}{A}\right).\arccos\left(\frac{A - (DX + C)}{A}\right) - \sqrt{1 - (\frac{A - (DX + C)}{A})^2}\right)$$

$$+ \frac{A^3}{3D}\left(\sqrt{1 - (\frac{DX + C - A}{A})^2})\right)^3 \ldots\ldots \text{Eq. A. 46}$$

Replacing A, D, C, and X (from Equation A.13) into Equation A.46 will result in Equation A.47. Note the boundaries should be replace the Z to achieve the final answer (note boundaries in Equation A.47).

$\mathrm{V}_c = \text{Cutter Volume}$

$$= \left\{ \frac{-\left(\frac{D_c}{2}\right)^3}{-Tan(BR)} \left[\left(\frac{\left(\frac{D_c}{2}\right) - \left(-Tan(BR)\, Z + \left(\frac{BG.D_c}{8}\right)\right)}{\left(\frac{D_c}{2}\right)} \right). \arccos \left(\frac{\left(\frac{D_c}{2}\right) - \left(-Tan(BR)\, Z + \left(\frac{BG.D_c}{8}\right)\right)}{\left(\frac{D_c}{2}\right)} \right) \right.\right.$$

$$\left.\left. - \sqrt{1 - \left(\frac{\left(\frac{D_c}{2}\right) - \left(-Tan(BR)\, Z + \left(\frac{BG.D_c}{8}\right)\right)}{\left(\frac{D_c}{2}\right)} \right)^2} \right]$$

$$+ \frac{\left(\frac{D_c}{2}\right)^3}{-3\,Tan(BR)} \left(\sqrt{1 - (\frac{-Tan(BR)\, Z + \left(\frac{BG.D_c}{8}\right) - \left(\frac{D_c}{2}\right)}{\left(\frac{D_c}{2}\right)})^2)} \right)^3 \Bigg\} \Bigg[\begin{matrix} Cot(BR).\left(\frac{BG.D_c}{8}\right) \\ 0 \end{matrix} \ldots\ldots \text{Eq. A. 47}$$

Replace the boundaries into Equation A.47 will result in Equation A.48.

$$V_c = \text{Cutter Volume}$$

$$= \frac{-\left(\frac{D_c}{2}\right)^3}{-Tan(BR)} \left[* \arccos\left(\frac{\left(\frac{D_c}{2}\right) - \left(-Tan(BR).Cot(BR).\left(\frac{BG.D_c}{8}\right) + \left(\frac{BG.D_c}{8}\right)\right)}{\left(\frac{D_c}{2}\right)} \right) - \sqrt{1 - \left(\frac{\left(\frac{D_c}{2}\right) - \left(-Tan(BR).Cot(BR).\left(\frac{BG.D_c}{8}\right) + \left(\frac{BG.D_c}{8}\right)\right)}{\left(\frac{D_c}{2}\right)} \right)^2} \right]$$

$$+ \frac{\left(\frac{D_c}{2}\right)^3}{-3\,Tan(BR)} \left(\sqrt{1 - \left(\frac{-Tan(BR).Cot(BR).\left(\frac{BG.D_c}{8}\right) + \left(\frac{BG.D_c}{8}\right) - \left(\frac{D_c}{2}\right)}{\left(\frac{D_c}{2}\right)} \right)^2} \right)^3$$

$$- \left[\frac{-\left(\frac{D_c}{2}\right)^3}{-Tan(BR)} \left[\left(\frac{\left(\frac{D_c}{2}\right) - \left(\left(\frac{BG.D_c}{8}\right)\right)}{\left(\frac{D_c}{2}\right)} \right) . \arccos\left(\frac{\left(\frac{D_c}{2}\right) - \left(\left(\frac{BG.D_c}{8}\right)\right)}{\left(\frac{D_c}{2}\right)} \right) - \sqrt{1 - \left(\frac{\left(\frac{D_c}{2}\right) - \left(\left(\frac{BG.D_c}{8}\right)\right)}{\left(\frac{D_c}{2}\right)} \right)^2} \right] \right.$$

$$\left. + \frac{\left(\frac{D_c}{2}\right)^3}{-3\,Tan(BR)} \left(\sqrt{1 - \left(\frac{\left(\frac{BG.D_c}{8}\right) - \left(\frac{D_c}{2}\right)}{\left(\frac{D_c}{2}\right)} \right)^2} \right)^3 \right] \quad \ldots\ldots\ldots \text{Eq. A. 48}$$

The cutter volume Equation is provided in the Equation A.49.

$$V_c = Cutter\ Volume = -\left[\frac{\left(\frac{D_c}{2}\right)^3}{Tan(BR)} \left[\left(\frac{\left(\frac{D_c}{2}\right) - \left(\frac{BG.D_c}{8}\right)}{\left(\frac{D_c}{2}\right)} \right) . arccos\left(\frac{\left(\frac{D_c}{2}\right) - \left(\frac{BG.D_c}{8}\right)}{\left(\frac{D_c}{2}\right)} \right) - \right. \right.$$

$$\left. \left. \sqrt{1 - \left(\frac{\left(\frac{D_c}{2}\right) - \left(\frac{BG.D_c}{8}\right)}{\left(\frac{D_c}{2}\right)} \right)^2} \right] - \frac{\left(\frac{D_c}{2}\right)^3}{3\,Tan(BR)} \left(\sqrt{1 - \left(\frac{\left(\frac{BG.D_c}{8}\right) - \left(\frac{D_c}{2}\right)}{\left(\frac{D_c}{2}\right)} \right)^2} \right)^3 \right] \quad \ldots\ldots\ldots Eq. A. 49$$

A.2 PDC and Carbide Worn Volume Calculations

The goal of this section is to find the PDC and carbide volumes. This section will expand on the volume calculations from appendix A.1.

A.2.1 If $L_{PDC} \geq L'$

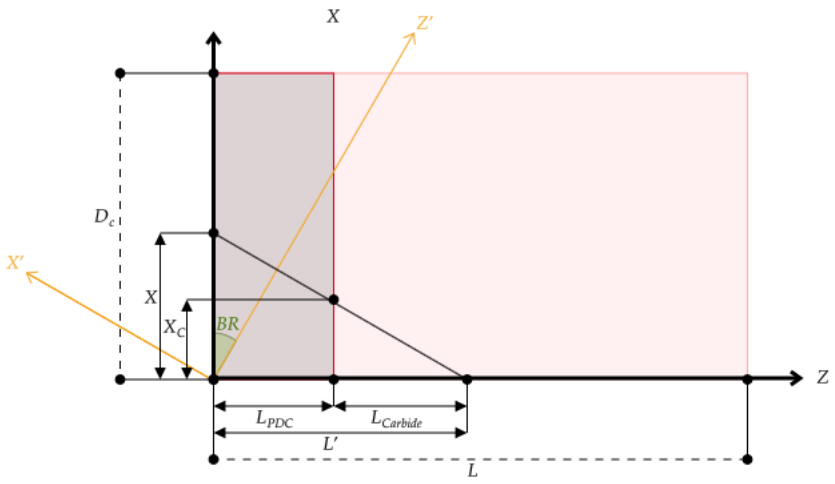

Figure A4. Cutter side view for PDC and carbide wear volumes

Figure A4 shows a cylinder (cutter) laid down on Z axis and L' has been split into two sections, L_{PDC} (darker shaded rectangle) and $L_{Carbide}$ (light shaded rectangle), to represent the length of wear for both materials. If L' is less that L_{PDC} then the carbide substrate has yet to be reached, in this case

$$\mathrm{L_{Carbide}} = 0 \ldots\ldots\ldots \mathrm{Eq.\,A.\,50}$$

$$\mathrm{V_{PDC}} = \mathrm{V_{Total}} \ldots\ldots\ldots \mathrm{Eq.\,A.\,51}$$

$$\mathrm{V_C} = 0 \ldots\ldots\ldots \mathrm{Eq.\,A.\,52}$$

A.2.2 $L_{PDC} < L'$

At the point that L' overcomes L_{PDC}, wear of the carbide substrate begins. The carbide portion of the cutter can be seen as a new cutter if the X-Z origin is shifted, in the positive Z direction, the length of L_{PDC} as seen in Figure A4.

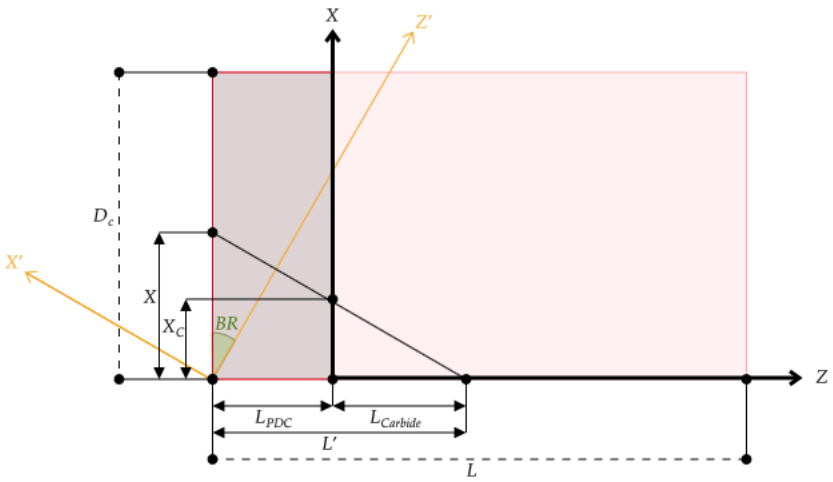

Figure A5. Cutter side view with X-Z origin shift

By shifting the X-Z origin, the volume of the carbide substrate can now be calculated by using the same equations from appendix A.1 if L' is replaced with $L_{Carbide}$.

To solve for $L_{Carbide}$, the diamond layer thickness or L_{PDC} must be known. L_{PDC} can be found in a bit catalog or from the cutter manufactured, often times the thickness is $.078 \pm .0008\ in.$ With the L_{PDC} and the L' from Eq. A.5

$$L_{Carbide} = L' - L_{PDC} \ldots\ldots\ldots \text{Eq. A. 53}$$

Rearranging the Eq. A.5, a function is formed for BG as a function of L'

$$BG = \frac{L' * 8}{\cot(BR) * D_c} \ldots\ldots\ldots \text{Eq. A. 54}$$

Replacing L' with $L_{Carbide}$ in Eq. 54 results in

$$BG_{Carbide} = \frac{L_{carbide} * 8}{\cot(BR) * D_c} \ldots\ldots\ldots \text{Eq. A. 55}$$

$BG_{Carbide}$ is the bit grade seen at the shifted X-Z origin and can now replace BG in Equation A.49, resulting in carbide volume removed from the cutter

$$V_{carbide} = -\left[\frac{\left(\frac{D_c}{2}\right)^3}{Tan(BR)}\left[\left(\frac{\left(\frac{D_c}{2}\right)-\left(\frac{BG_{Carbide}.D_c}{8}\right)}{\left(\frac{D_c}{2}\right)}\right).arccos\left(\frac{\left(\frac{D_c}{2}\right)-\left(\frac{BG_{Carbide}.D_c}{8}\right)}{\left(\frac{D_c}{2}\right)}\right)\right.\right.$$

$$\left.\left.-\sqrt{1-\left(\frac{\left(\frac{D_c}{2}\right)-\left(\frac{BG_{carbide}.D_c}{8}\right)}{\left(\frac{D_c}{2}\right)}\right)^2}\right]\right.$$

$$\left.-\frac{\left(\frac{D_c}{2}\right)^3}{3\,Tan(BR)}\left(\sqrt{1-\left(\frac{\left(\frac{BG_{carbide}.D_c}{8}\right)-\left(\frac{D_c}{2}\right)}{\left(\frac{D_c}{2}\right)}\right)^2}\right)^3\right] \ldots\ldots..Eq.A.56$$

With both the $V_{carbide}$ and V_{Total}, the PDC volume removed from the cutter can be found

$$V_{PDC} = V_{Total} - V_{carbide} \ldots\ldots..Eq.A.57$$

VITA

Douglas Brock Bridges

Candidate for the Degree of

Master of Science

Thesis: CUTTER WEAR AND TEMPERATURE MODELING

Major Field: Petroleum Engineering

Biographical:

Education:

Completed the requirements for the Master of Science in Petroleum Engineering at Oklahoma State University, Stillwater, Oklahoma in May, 2020.

Completed the requirements for the Bachelor of Science in Mechanical Engineering at Oklahoma State University, Stillwater, Oklahoma in May, 2018.

Experience:

Research Assistant, Oklahoma State University, Aug. '18 – May '20
- Develop a real-time drilling optimization system for geothermal drilling

Reservoir Engineering Intern, Chesapeake Energy Corp., May '19- Aug. '19
- Analyzed historic wells and recommended methods to boost production

Project Manager, Mach Energy Services, Nov. '16 – Jan. '17
- Communicated with staff and subcontractors to complete projects

Office Support, Courtney Construction, June '14 – Nov. '16
- Designed and implemented new methods to track job progress reporting

Professional Memberships:

- Society of Petroleum Engineers - Graduate Student Representative
- American Association of Drilling Engineers
- Tau Beta Pi Engineering Honor Society